JOURNAL OF COMPUTATIONAL PHYSICS 57, 90–128 (1985)

Computer-Aided Analysis of the Convergence to Steady State of Discrete Approximations to the Euler Equations

LARS E. ERIKSSON AND ARTHUR RIZZI

FFA The Aeronautical Research Institute of Sweden, S–161 11 Bromma, Sweden

Received July 12, 1983; revised February 21, 1984

The behaviour of a centered finite volume scheme for the isoenergetic Euler equations in two space dimensions is studied by numerical differentiation and approximate eigensystem analysis. The entire semidiscrete approximation including boundary conditions is formulated as a large system of ODEs, which are linearized by numerically approximating the Frechét derivative. An approximate eigensystem procedure that only needs the Frechét derivative is used to extract the least damped eigenmodes. The overall method has been applied to the case of transonic flow past an airfoil and has revealed that the most persistent transient modes are highly structured and are associated with eigenvalues of small modulus. Furthermore, they appear to be centered around the shock region, the stagnation region and the trailing edge/wake region of the airfoil. The beneficial effect of local time-step scaling and artificial dissipation is also demonstrated by the method.

1. INTRODUCTION

There is currently much activity in the development of a numerical method whose time iterations converge rapidly to the steady state of the compressible Euler equations which govern transonic flow. Recent years have seen the truly phenomenal success that the multigrid method has brought to the solution of elliptic equations, but despite a number of attempts to use it for the hyperbolic Euler equations no outstanding success has been reported yet. A substantial theory has arisen that explains why the method is so successful on elliptic systems but has not developed far enough to give us a clear understanding of its impotency with multidimensional hyperbolic systems. One lead towards a credible explanation focusses on the decomposition of the transient error that remains after application of the smoothing operator in the fine grid [1]. If the error is not sufficiently smooth, it is thought that the conventional multigrid method will not be effective. The general suspicion is that the persistent error modes which spring from eigenvalues of low modulus probably contain high spatial frequencies. Our own previous work [2] with a projection method, which is closely related to the multigrid concept, is a good example; during the early part of the convergence process our method had some effect in reducing the

0021-9991/85 $3.00

residual error, but as the steady state was approached it ceased to act on the remaining error. Such findings beg for analysis to help us understand the behaviour of the equations we are trying to solve.

Any theory with which to study the problem must necessarily be based on a locally linear analysis of the discretized Euler equations, but we deem it unwise to make further simplifications in the equations or in the number of spatial dimensions, so we treat them in their entirety. The discrete model that we choose to study is the centered finite volume scheme in two-space dimensions, which is also the model that we used in our previous attempt at multigrid by projection [2]. Two different types of dissipation are used, a nonlinear (solution-dependent) dissipation acting primarily in regions with rapid variation and a linear dissipation to damp spurious solutions. The particular flow case used for this analysis is the transonic flow about an airfoil, so we apply absorbing boundary conditions at the outer boundary. We prefer to formulate the scheme as being continuous in time and discrete in space, i.e., a semidiscrete approximation, and the time integration is then approximated by a multi-stage predictor-corrector type of scheme.

Viewing the complete semidiscrete approximation to the Euler equations as a large system of first-order ODEs, it is evident that a local linearization of these equations gives us a large linear system whose eigenvalues and eigenvectors determine the local time evolution of the system. If the system is dissipative and converges towards a unique steady solution, it is also clear that it is the properties of the linearized system that determine the asymptotic rate of convergence.

Clearly the analysis of such a large and complicated linear system cannot be accomplished by analytic means. Lomax [1], however, has advanced the analysis significantly by using the computer to calculate numerically the eigenvalues of the matrix that he formulated analytically from a one-dimensional system. His approach relies on standard eigenvalue-computing routines and is limited necessarily to one-dimensional systems since these routines are applicable for matrices up to at most order 200.

The purpose of this paper is to advance this type of eigensystem analysis by computer a step beyond what Lomax did in two particular aspects. Rather than form the matrix of the system analytically by hand, which is easy to do at interior points of the domain but very tedious at boundaries and for nonlinear dissipation terms, we use the computer to linearize our system by numerically approximating the so-called Frechét derivative. The second novel feature of this paper is the approximation technique we use to compute eigenvalues and eigenvectors of large nonsymmetric matrices, which enables us to study the Euler equations in two-space dimensions without compromise. This eigenvalue approximation technique was originally developed to investigate the effects of mesh singularities on finite difference schemes for hyperbolic equations [3], but turned out to be ideally suited for this application also.

We demonstrate the power of this analysis procedure first by showing how the well-known technique of scaling the equations by the local time-step [4] produces a much improved conditioning of the system. A second investigation shows the

unstable behaviour of the equations without the addition of any artificial viscosity and also the stabilizing effect of first only nonlinear dissipation and then a combination of nonlinear and linear dissipation. But the main goal of our analysis is to unveil the nature and character of the persistent transient modes that determine the asymptotic convergence to steady state. Our findings on three successive meshes, a coarse (32×7) mesh, a medium (64×14) mesh and a fine (128×28) 0-type mesh show that the most persistent modes are nonspurious in the sense that they seem to approximate some physical properties of the flow and furthermore they are associated with eigenvalues of very small modulus. What is striking about these modes, unlike those found in elliptic problems, is their complex structure, a feature that would call into question the ability of any conventional multigrid method to work effectively on them. This structure is centered around the shock region, the stagnation region and the trailing edge/wake region of the airfoil. Further details of the analysis method and a discussion of our findings are elaborated upon in the following paragraphs.

2. Method of Analysis

2.1. *Linearization*

The large system of ODEs that is obtained when semidiscretizing the Euler equations in two-space dimensions, can in principle be linearized analytically, but in practice this is very difficult due to the complicated boundary conditions (of absorbing type) and the use of nonlinear artificial dissipation. Since we do not want to make any more simplifications than the linearization, we choose to differentiate the system numerically. For a given system defined by

$$u_t = f(u) \tag{1}$$

where $u = [u_1,..., u_n]^T$ and $f = [f_1,..., f_n]^T$, we can perturb the argument of f by an arbitrary vector $d = [d_1,..., d_n]^T$ and thereby obtain the Frechét derivative of f as the limit

$$\lim_{\varepsilon \to 0} \frac{1}{\varepsilon} (f(u + \varepsilon d) - f(u)) = \frac{df}{du} \cdot d. \tag{2}$$

It is evident that (2) can be used to approximate $(df/du) \cdot d$ numerically by choosing a small but nonzero value of ε. However, a better approximation is obtained by central differences as in the second-order accurate scheme

$$\frac{df}{du} \cdot d \approx \frac{1}{2\varepsilon} (f(u + \varepsilon d) - f(u - \varepsilon d)) \tag{3}$$

or as in the fourth-order accurate scheme

$$\frac{df}{du} \cdot d \approx \frac{1}{12\varepsilon} (-f(u + 2\varepsilon d) + 8f(u + \varepsilon d) - 8f(u - \varepsilon d) + f(u - 2\varepsilon d)). \tag{4}$$

As in all numerical differentiation schemes, the choice of ε should be such that a reasonable balance between truncation error and roundoff error is obtained. In our case, extensive experimenting and checking led us to choose the fourth-order accurate scheme (4) implemented in double precision and ε such that $\|\varepsilon d\|/\|u\| = 0.001$ (using the L_2 norm $\|u\|^2 = u^T u$).

In principle, the numerical differentiation schemes (2), (3), (4) can be used to compute the complete Jacobian matrix df/du by setting the perturbation vector to

$$d_k = (0,..., 0, \underset{\substack{\uparrow \\ k^{\text{th}} \text{ element}}}{1}, 0,..., 0)^T \tag{5}$$

and computing the k^{th} column of df/du by

$$k^{\text{th}} \text{ column of } \frac{df}{du} = \frac{df}{du} \cdot d_k \tag{6}$$

for $k = 1,..., n$. However, considering that the systems we want to analyze have of the order of 10^3 to 10^4 variables, it is clear that the computation and storage of the complete matrix df/du is not practical. Furthermore, the use of standard numerical eigenvalue algorithms to compute the complete spectrum of df/du is also out of the question for such large systems. We are therefore forced to use a method that is capable of extracting a subset of the total spectrum and that only needs the Frechét derivative $df/du \cdot d$ for arbitrary vectors d to accomplish this. The method that we choose to use actually consists of two parts, a method for approximate eigenvalue analysis and a method for transforming the spectrum of an arbitrary matrix. Both of these methods are described in the following paragraphs.

2.2. *Approximate Eigenvalue Analysis*

The core of the eigenvalue analysis algorithm is Arnoldi's method [5], which is a Krylov subspace method. We describe the method briefly. An approximate solution to the eigenvalue problem

$$Au = \lambda u \tag{7}$$

where A is an $n \times n$ matrix and u is an $n-$ vector, is constructed by constraining the solution vector u to the Krylov subspace K_m defined by

$$\begin{aligned} K_m &= \text{span } \{p_1, p_2,..., p_m\} \\ p_1 &\text{ given starting vector} \\ p_{k+1} &= Ap_k \qquad k = 1, 2,..., m-1; m \ll n \end{aligned} \tag{8}$$

and requiring that the residual of (7) be orthogonal to K_m. This is accomplished by the algorithm

$$
\begin{aligned}
&p_1 \text{ given starting vector}\\
&e_1 = (p_1^T p_1)^{-1/2} p_1\\
&\text{for } k = 1 \text{ to } m:\\
&\quad p_{k+1} = A e_k - \sum_{j=1}^{k} h_{j,k} e_j; \qquad h_{j,k} = e_j^T A e_k\\
&\quad h_{k+1,k} = (p_{k+1}^T p_{k+1})^{1/2}\\
&\quad e_{k+1} = (h_{k+1,k})^{-1} p_{k+1}\\
&\text{next } k
\end{aligned}
\tag{9}
$$

where the coefficients $h_{j,k}$ define an upper Hessenberg matrix H_m. The eigenvalues of H_m are the desired approximate eigenvalues of A and the eigenvectors of H_m define the corresponding approximate eigenvectors of A:

$$
\begin{aligned}
H_m v_j &= \tilde{\lambda}_j v_j, && j = 1,\ldots, m\\
\tilde{u}_j &= \sum_{k=1}^{m} (v_j)_k e_k, && j = 1,\ldots, m
\end{aligned}
\tag{10}
$$

It has been shown [6] that the accuracy of the approximate spectrum obtained is best for the outer parts of the spectrum of A whereas the inner parts are poorly represented. This means that the approximate eigenvalue method must be used together with a spectrum transformation algorithm that is capable of moving the interesting parts of the spectrum outwards.

2.3. *Spectrum Transformation*

Since we are particularly interested in the asymptotic convergence of the system (1), we want to obtain good approximations to those eigenvalues λ_A of $A = df/du$ that have small negative real parts. In order to accomplish this with Arnoldi's method we must find a matrix transformation $C = g(A)$ such that the interesting part of A's spectrum is mapped to the outer part of C's spectrum. The obvious choice in this case is the transformation $C(t) = e^{tA}$ (where t is an arbitrary real and positive constant) which maps the left half of A's eigenvalue plane to the interior of the unit circle in C's eigenvalue plane. From the corresponding spectrum transformation $\lambda_C = \exp(t\lambda_A)$ we see that now it is the largest eigenvalues of $C(t)$ that we desire. For practical reasons we can only compute polynomial approximations of $C(t)$ as, for example, the second-order accurate Gary [7] approximation ($t = l\,\Delta t$)

$$
C(t) \approx D(\Delta t, l) = (I + \Delta t\, A + \tfrac{1}{2}\Delta t^2 A^2 + \tfrac{1}{4}\Delta t^3 A^3)^l \tag{11}
$$

or the fourth-order accurate Runge–Kutta approximation

$$C(t) \approx D(\Delta t, l) = (I + \Delta t A + \tfrac{1}{2}\Delta t^2 A^2 + \tfrac{1}{6}\Delta t^3 A^3 + \tfrac{1}{24}\Delta t^4 A^4)^l \tag{12}$$

which only involve powers of the matrix A. Since Arnoldi's method applied to $D(\Delta t, l)$ only requires the product $D(\Delta t, l)u$ for arbitrary n-vectors u it is evident that polynomial approximations like (11) or (12) can be evaluated by Horner's scheme and thus only involve the product Au for arbitrary n-vectors u. As described in Section 2.1 the product $Au = df/du \cdot u$ can then be approximated by a difference scheme such as (4). Since (11) and (12) are well-known explicit time-integration schemes with time-step Δt, we know that Δt is limited by the condition that all eigenvalues $\Delta t \lambda_A$ of the matrix $\Delta t A$ which satisfy $\mathrm{Re}(\Delta t \lambda_A) \leqslant 0$ must fall within the region of absolute stability. For the rest of this paper we will refer to this maximum time step as $\Delta t_{\max}$. Although the region of absolute stability of (12) is larger than that of (11), we have chosen scheme (11) for the practical reason that it requires less computer storage. A simple algorithm to compute $D(\Delta t, l)u$ is then

u arbitrary n-vector
for $k = 1$ to l:
$u_0 := u$
$u := u_0 + \frac{1}{2}\Delta t A u$
$u := u_0 + \frac{1}{2}\Delta t A u$
$u := u_0 + \Delta t A u$
next k
$D(\Delta t, l)u := u$ (13)

The function of l in (13) is to determine the "selectivity" of the transformation. As l increases, the spectrum of $D(\Delta t, l)$ "collapses" more and more into the point $\lambda_D = 0$ and the relative separation of the largest eigenvalues increases. This means that for sufficiently large l, Arnoldi's method can resolve the largest eigenvalues of $D(\Delta t, l)$ with $m \ll n$. Since the eigenvectors of A and $D(\Delta t, l)$ are identical it is clear that we can obtain the least damped eigenvectors of A with this technique.

3. Artificial Viscosity Model

All discrete methods to solve the Euler equations are dissipative at the level of their truncation error, if not across the entire spectrum of scales then at least for the higher frequency range. While some difference schemes are inherently dissipative others are not, or not to a sufficient degree, but they can be made dissipative by adding to the convective difference a damping term whose magnitude lies in the range of the truncation error of the discrete approximation. This is the so-called artificial viscosity

model, the rationale for which can be argued on numerical as well as physical grounds. Centered differences suffer from nonlinear aliasing effects, and when shock waves are to be captured all schemes, no matter the type, require some form of entropy condition to make the solution unique. But even if the flow is smooth the existence and uniqueness of a steady-state solution to the Euler equations cannot be taken for granted. In nonlinear transport there is a mechanism by which energy migrates from long-wavelength motion to progressively shorter and shorter scales until in reality it is removed from the flow by molecular viscosity. The differential Euler equations possess no such viscosity so that this energy can pile up in the small scales. But in the discrete representation it migrates to the smallest scale resolveable on the mesh and then returns transformed to large-scale motion via aliasing, which clearly is nonphysical and would appear to make a steady state unattainable. Within the context of the inviscid flow equations, the usual recourse to all of these deficiencies, albeit crude, is to attenuate waves more and more severely as their wavelength decreases so that none migrate out and alias back, but in such a way as not to alter completely the inviscid character of the solution. The idea of course is to model the short-wave dissipation by the real physical viscosity, and its justification is simply that in inviscid flow short-wave motion is of such low amplitude that whether removed or not it has no important effect on the overall flow character. In actual flow simulations this model is judged qualitatively with a view to the crispness of shock profiles and the thinness of vortex sheets in weak solutions, and the amount of entropy produced or equivalently the variation in total pressure through regions of smooth flow.

A large literature is developing on the construction of such artificial viscosity models, but the degree and character of damping that is applied varies in detail from method to method, and is quite arbitrary except for classification according to its order of magnitude in terms of mesh spacing. What is lacking in the judgement of these models is a quantitative assessment of their effects, and it is precisely here that we think our eigenmode analysis can provide some fresh insight because it takes into account all of the minute details of the individual model such as nonlinear switches and even boundary conditions.

We choose to introduce our dissipation model into the system at the same time level as the transport process. Our total difference operator $f(u)$ therefore consists of (1) the convective part $f_c(u)$ that results from discretizing the Euler equations in space by the centered finite-volume scheme, adding the appropriate boundary conditions, and then scaling it with the local time step, and (2) the dissipative part $f_D(u)$. The semidiscrete approximation (1) can then be written

$$u_t = f_C(u) + f_D(u) = f(u). \tag{14}$$

The total discrete dissipative operator $f_D(u)$ includes the boundary conditions and is composed of both linear and nonlinear terms according to $f_D(u) = g(u) + Du$ where D is a constant matrix. The nonlinear expression is designed to provide dissipation at discontinuities whereas the linear one is formulated to suppress spurious solutions (sawtooth waves) and to control the migration of energy from large to subgrid scales.

3.1. *Nonlinear Artificial Viscosity*

Let $u_{j,k}$ denote the discrete solution in the jkth cell and define the central difference operators δ_J and δ_K by

$$\delta_J u_{j,k} = u_{j+1/2,k} - u_{j-1/2,k}; \qquad \delta_K u_{j,k} = u_{j,k+1/2} - u_{j,k-1/2}.$$

For all cells in the interior of the domain the nonlinear artificial viscosity is expressed by

$$g_{j,k} = (\delta_J \varepsilon_{j,k}(u)\, \delta_J + \delta_K \alpha_{j,k}(u)\, \delta_K)\, u_{j,k} \tag{15}$$

where $\varepsilon_{j,k}$ and $\alpha_{j,k}$ are coefficients that depend on the solution field according to $\varepsilon_{j,k} \sim |\delta_J^2 p_{j,k}|$ and $\alpha_{j,k} \sim |\delta_K^2 p_{j,k}|$ where $p_{j,k}$ is the pressure in cell jk. These coefficients sense nonsmooth flow and increase the filtering of large gradients so that in effect an entropy condition is enacted. This much is standard and is used in many methods. However, at cells adjacent to boundaries outside of which $u_{j,k}$ cannot be defined naturally, expression (15) must be modified, and here enters a degree of arbitrariness that causes the results of one method to differ markedly from another. We believe that the quadratic form $u^T Hu$, where $Hu = g(u)$ for fixed $\varepsilon_{j,k}, \alpha_{j,k}$, provides a useful guideline for the appropriate choice at such boundaries. The purpose of the total dissipative operation is to drain off energy as time increases. At boundaries if we simply set the corresponding sensor α or ε in Eq. (15) to zero we find that the quadratic form

$$u^T Hu = \sum_{j=1}^{NJ} \sum_{k=1}^{NK} u_{j,k} H u_{j,k} = - \sum_{j=1}^{NJ-1} \sum_{k=1}^{NK} \varepsilon_{j+1/2,k}(u_{j+1,k} - u_{j,k})^2 - \sum_{j=1}^{NJ} \sum_{k=1}^{NK-1} \alpha_{j,k+1/2}(u_{j,k+1} - u_{j,k})^2$$

is always negative and hence energy dissipates even in the boundary cells.

3.2. *Linear Artificial Viscosity*

We have studied two alternative models for linear artificial viscosity. The first one,

$$Du_{j,k} = \varepsilon(\delta_J^2 + \delta_K^2)\, u_{j,k} \tag{16}$$

stems from Eq. (15) by taking $\varepsilon_{j,k} = \alpha_{j,k} = \varepsilon = \text{constant}$. The second alternative uses the fourth-difference operator

$$Du_{j,k} = -\varepsilon(\delta_J^4 + \delta_K^4)\, u_{j,k} \tag{17}$$

at all interior cells. But at boundaries we must alter this expression, and we seek to do so in a way that guarantees positive dissipation in all cells. Guided again by its quadratic form we use no data outside the computational domain but instead incorporate noncentered differences for the boundary cells together with scheme (17) at the

interior ones in order to obtain the total discrete linear dissipative operator D with the property

$$\begin{aligned} u^T Du &= \sum_{j=1}^{NJ} \sum_{k=1}^{NK} u_{j,k} Du_{j,k} \\ &= -\varepsilon \sum_{j=2}^{NJ-1} \sum_{k=1}^{NK} (u_{j+1,k} - 2u_{j,k} + u_{j-1,k})^2 \\ &\quad -\varepsilon \sum_{j=1}^{NJ} \sum_{k=2}^{NK-1} (u_{j,k+1} - 2u_{j,k} + u_{j,k-1})^2 \end{aligned} \tag{18}$$

which automatically ensures that the dissipation is greater than or equal to zero (for $\varepsilon > 0$). The attractive feature of this artificial viscosity model, easily seen in Eq. (18), is that if $u_{j,k}$ is bilinear in j and k the total operator D acting on $u_{j,k}$ always returns zero, even at the boundaries. Compare this to the second-difference operator H that gives a zero result only if $u_{j,k}$ is a constant. The details of the construction of D will be presented in a forthcoming paper.

4. Findings from the Analysis

In order to build confidence in and gain an appreciation for the things one can learn with this analysis tool we begin with a study of some common aspects of numerical methods whose effects are well known, the local time-step scaling and the addition of artificial viscosity. Then in a way not possible before we go on to cast new light on the problem of slow convergence to a steady-state solution, the main theme of the paper.

4.1. *Initial Results for Method Validation*

As a demonstration of the capabilities of our analysis method we first show the effect of the well-known (but not thoroughly analyzed) local time-step scaling [4] on the conditioning of the linearized system. Choosing a 32×7 mesh around a NACA 0012 airfoil and advancing the fully nonlinear system in time from an initial freestream solution at $M_\infty = 0.8$, $\alpha = 0°$, we stop after a relatively short time (15 time steps) and analyze the linearized system. The solution at this instant is far from steady state and is dominated by waves travelling outwards from the airfoil. The approximate spectrum obtained for this linear system without any spectrum transformation is shown in Fig. 1a, both with and without local time-step scaling. As mentioned in Section 2.2, the Arnoldi method needs a starting vector p_1 to define the Krylov subspace, and in this case we use random vectors. In each spectrum, the results for three different starting vectors are shown, and the spread of the approximate eigenvalues gives an indication of the error or uncertainty. The interesting feature in these spectra is the fact that the unscaled system seems to have an eigenvalue very near the origin; i.e., it is very nearly singular. In order to confirm this near

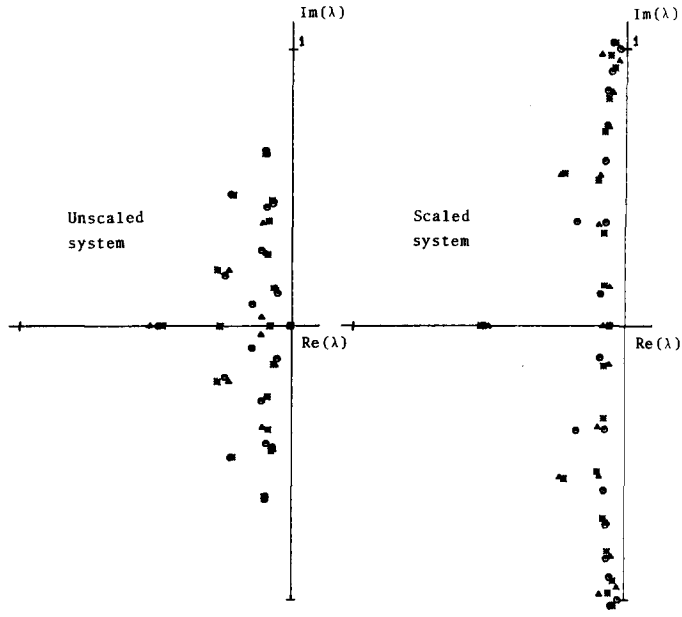

FIG. 1a. Effect of local time-step scaling on spectrum of linearized system. 32×7 grid around NACA 0012 airfoil, $M_\infty = 0.8$, $\alpha = 0°$, nonlinear dissipation added. System linearized after 15 time steps with free-stream initial conditions.

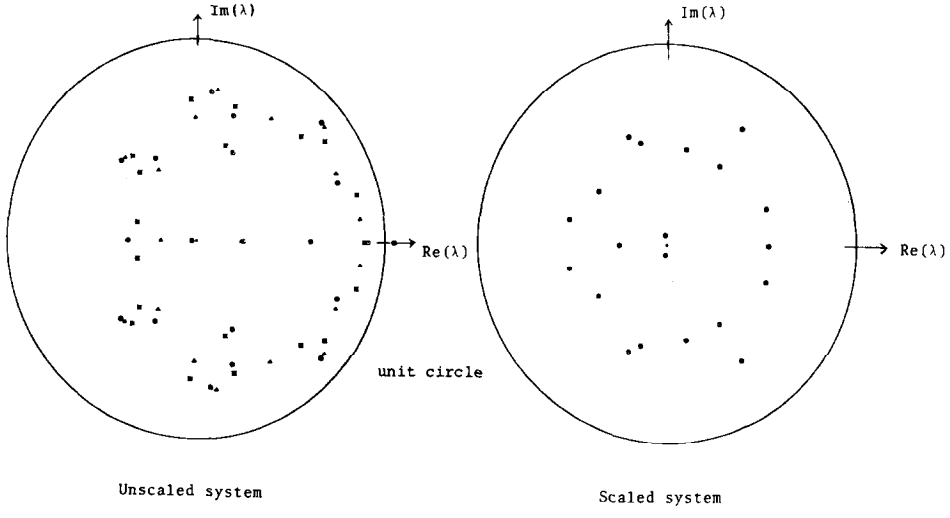

FIG. 1b. Effect of local time-step scaling on spectrum of transformed linearized system. Transformation defined by $D(\Delta t, l) = (I + \Delta t A + \frac{1}{2}\Delta t^2 A^2 + \frac{1}{4}\Delta t^3 A^3)^l$ for $\Delta t = 0.9\Delta t_{\max}$, $l = 20$. Otherwise the same case as in Fig. 1a.

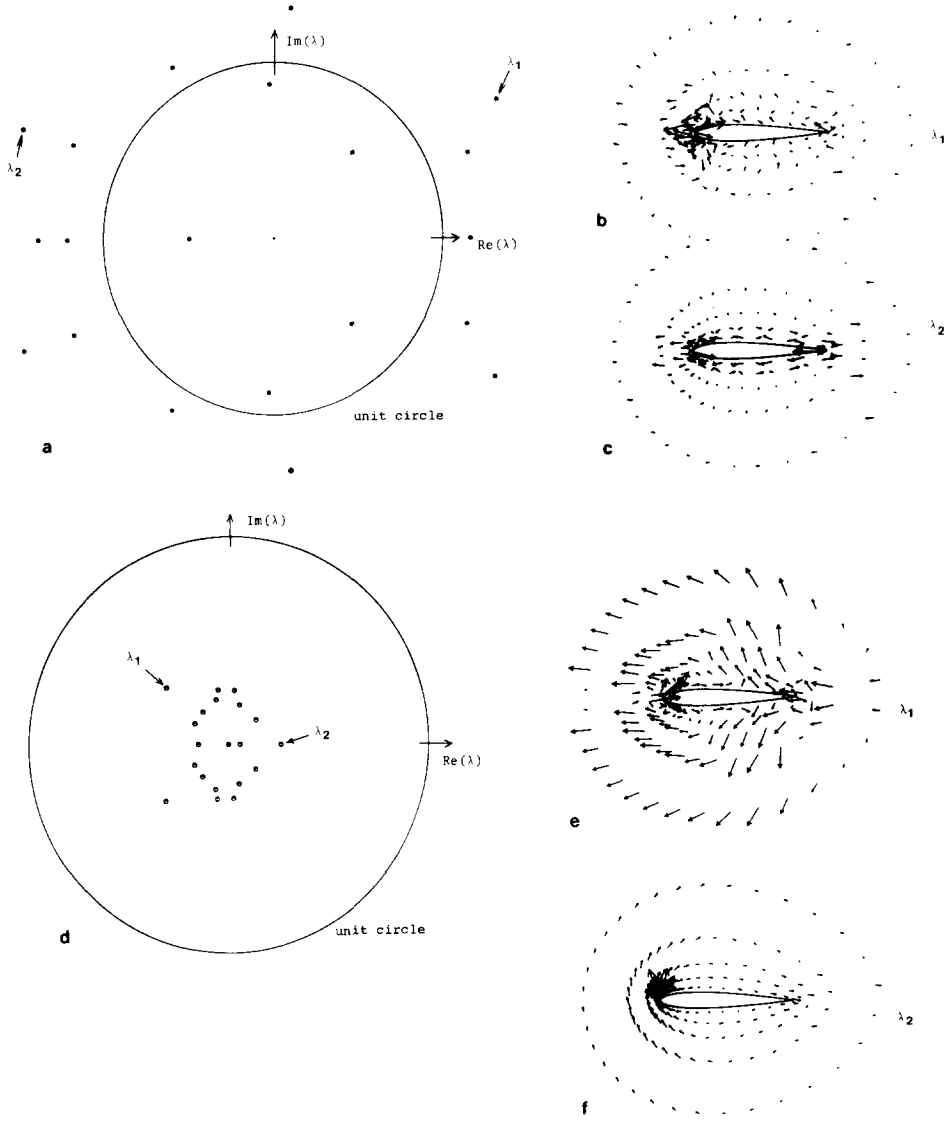

FIG. 2a. Spectrum of transformed linearized system. Transformation defined by $D(\Delta t, l) = (I + \Delta t A + \frac{1}{2}\Delta t^2 A^2 + \frac{1}{4}\Delta t^3 A^3)^l$ for $\Delta t = 0.9\Delta t_{\max}$, $l = 50$. 32×7 grid around NACA 0012 airfoil, $M_\infty = 0.8$, $\alpha = 0°$, local time-step scaling, *no dissipation*. System linearized after 15 time steps with free-stream initial conditions.

FIG. 2b, c. Imaginary part of eigenmodes associated with eigenvalues 1 and 2 in Fig. 2a. Eigenmodes visualized by plotting x, y-components of momentum as vectors emanating from corresponding mesh points.

FIG. 2d. Same case as in Fig. 2a except that nonlinear dissipation is added.

FIG. 2e, f. Real part of eigenmodes associated with eigenvalues 1 and 2 in Fig. 2d.

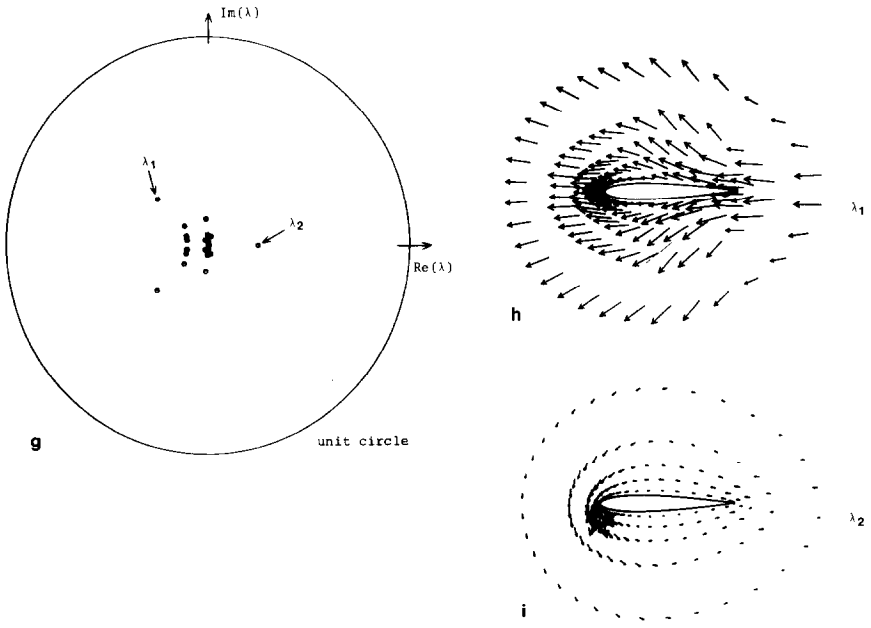

FIG. 2g. Same case as in Fig. 2a except that both non-linear and linear dissipation is added.

FIG. 2h, i. Real part of eigenmodes associated with eigenvalues 1 and 2 in Fig. 2g.

singularity, we compute the corresponding spectrum of the transformed matrix $D(\Delta t, l)$ described in Section 2.3 with $\Delta t = 0.9\Delta t_{\max}$ and $l = 20$, which gives us a considerably improved resolution of the region around the origin of the original eigenvalue plane (corresponding to the region around the point 1 in the spectrum of $D(\Delta t, l)$). As can be seen in Fig. 1b, the near singularity of the unscaled system is confirmed and the much improved conditioning due to the local time-step scaling is quite clear.

Next we show the effect of the artificial viscosity on the eigenvalues and eigenvectors of the linearized system. Three different cases are compared with each other; no dissipation added, only nonlinear dissipation added, and both nonlinear and linear dissipation added. In all three cases, we first advance the fully nonlinear system 15 time steps (starting with the freestream solution) and then analyze the resulting linearized system. The eigenvalues and some eigenvectors of the corresponding $D(\Delta t, l)$-matrices for $\Delta t = 0.9\Delta t_{\max}$ and $l = 50$ are shown in Figs. 2a–i. The eigenmodes are visualized by plotting the x and y momentum components of the eigenmodes as vectors emanating from the corresponding mesh points. As expected, the first case with no added dissipation displays several unstable modes and the two typical eigenmodes shown have the characteristic plus-minus pattern of spurious modes (Figs. 2a, b, c). By adding the nonlinear dissipation to the system, we see that the unstable modes disappear and the eigenmodes corresponding to the least damped

eigenvalues have a much more coherent structure (Figs. 2d, e, f). Finally, the addition of a global linear dissipation seems to damp the more irregular modes further so that the most persistent modes now look very smooth (Figs. 2g, h, i). The results indicate that the global linear dissipation is a valuable complement to the standard nonlinear dissipation.

4.2. *Asymptotic Convergence*

Having established the validity of the analysis procedure, we now turn to the main objective of this paper, the study of eigenvalues and eigenvectors of the linearized system near the steady state solution. As mentioned previously, it is these eigenvalues and eigenvectors that govern the asymptotic convergence of the semidiscrete approximation to steady state. The first question that we want to answer is what eigenvalues are responsible for the asymptotic convergence rate of our overall method. Since the spatial discretization is centered, the spectrum is dominated by complex eigenvalues with large imaginary parts and small real parts and it is therefore not immediately clear whether it is large modulus or small modulus eigenvalues that dictate the asymptotic convergence rate.

As a typical example we show the spectrum obtained for a medium mesh case. Advancing the fully nonlinear system 500 time steps (after which the solution can be considered stationary) on a 64×14 mesh around the NACA 0012 airfoil from a freestream initial solution at $M_\infty = 0.8$, $\alpha = 0°$, we linearize and compute the approximate spectrum of this linear system (Fig. 3a). Both nonlinear and linear artificial viscosity (of the second-difference type) is used in this case. The approximate spectrum shown indicates that there are some eigenvalues very near the origin of the eigenvalue plane and this is confirmed by the spectrum of the corresponding $D(\Delta t, l)$-matrix for $\Delta t = 0.9\Delta t_{\max}$ and $l = 1$ (Fig. 3b). The transformed imaginary axis of the original eigenvalue plane is here indicated by the dashed line and it is quite clear that the least damped eigenvalues are to be found near the origin of the original eigenvalue plane. Very similar results have been obtained for both coarser (32×7) and finer (128×28) meshes. Furthermore, using a linear artificial viscosity of fourth-difference type instead of second-difference type does not affect this basic result.

The fact that the most persistent transient modes near steady state are associated with complex eigenvalues of small modules makes it natural to investigate the structure of these eigenmodes in the hope that they are smooth enough to make a projection onto a coarser mesh feasible, in the spirit of the multi-grid technique for elliptic problems. The faster convergence on the coarser mesh would then hopefully increase the overall convergence rate. However, it is not only the smoothness of the eigenmodes on a certain fixed mesh that is important in this context. The basic underlying assumption made in the multi-grid concept is that all of the most persistent eigenmodes in a particular mesh have very similar counterparts in the next coarser mesh. Obviously, it the eigenmodes are very smooth this will almost certainly be true, since the truncation error of the discrete approximation is small in that case. If, however, the eigenmodes on a given mesh show a very detailed structure that already is at the limit of what that particular mesh can resolve, it is very likely that

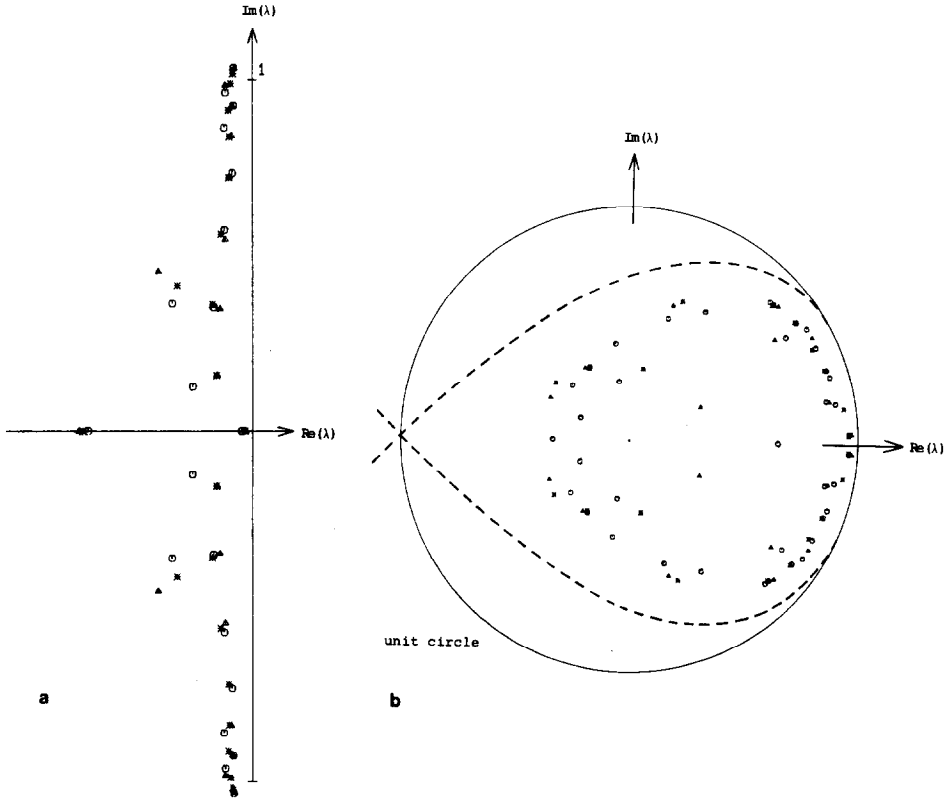

FIG. 3a. Spectrum of linearized system on a 64×14 mesh around the NACA 0012 airfoil at $M_\infty = 0.8$ and $\alpha = 0°$ with both nonlinear and linear artificial viscosity (of second-difference type) added. The system is linearized around a nearly steady solution (after 500 time steps).

FIG. 3b. Spectrum of transformed linearized system for the same case as in Fig. 3a. Transformation defined by $D(\Delta t, l) = (I + \Delta t A + \frac{1}{2}\Delta t^2 A^2 + \frac{1}{4}\Delta t^3 A^3)^l$ for $\Delta t = 0.9\Delta t_{\max}$, $l = 1$. Dashed line indicates the imaginary axis of the original eigenvalue plane.

the next coarser mesh will not have very similar counterparts of these modes. Projecting the persistent modes down to this coarser mesh could then easily result in a slowdown instead of an acceleration of the overall convergence. It is therefore important to study the structure of the most persistent eigenmodes not only on one single mesh but on a sequence of meshes.

The results that are presented in the following paragraphs have all been obtained for the NACA 0012 airfoil using either a coarse (32×7), a medium (64×14), or a fine (128×28) mesh. For all three meshes, the fully nonlinear system has been advanced 500 time steps, starting from a freestream initial solution in the coarse mesh case and from a solution interpolated from the next coarser mesh in the medium and fine mesh cases. The flow case chosen was $M_\infty = 0.8$, $\alpha = 0°$ as before and two different artificial viscosity models were used. The first model is the second-difference

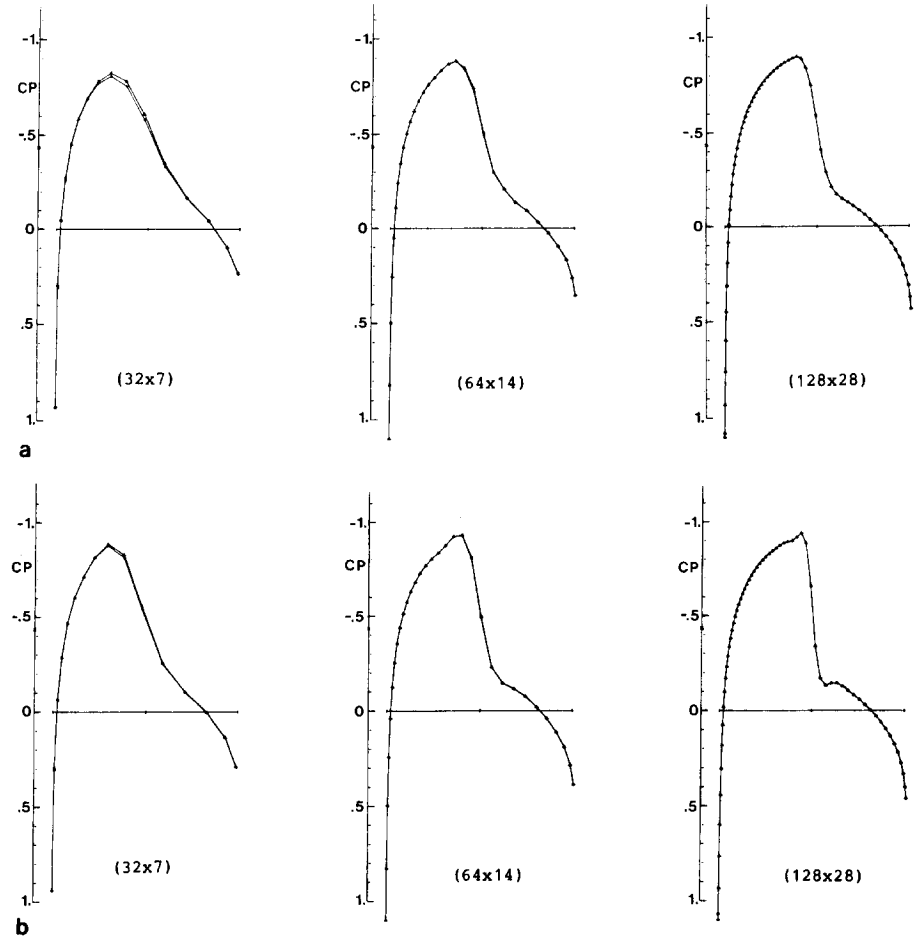

FIG. 4a. Pressure distributions for the solutions on which the linearization and eigensystem analysis was applied. NACA 0012 airfoil, 0-type mesh, $M_\infty = 0.8$, $\alpha = 0°$, nonlinear and linear second-difference type dissipation, 500 time steps on each mesh.

FIG. 4b. Pressure distributions for the solutions on which the linearization and eigensystem analysis was applied. NACA 0012 airfoil, 0-type mesh, $M_\infty = 0.8$, $\alpha = 0°$, nonlinear second-difference type and linear fourth-difference type dissipation, 500 time steps on each mesh.

nonlinear + second-difference linear combination and the second model is the second-difference nonlinear + fourth-difference linear combination (as described in Section 3). This resulted in six different steady solutions upon which the present analysis method was applied. The solutions are shown in Fig. 4 and differ mainly in the shock sharpness due to the different viscosity models. The approximate spectra of the $D(\Delta t, l)$-matrices for the six cases using $\Delta t = 0.9\Delta t_{\max}$ and $l = 50$ are presented in Figs. 5a–c and show that the effect of the two different artificial viscosity models on

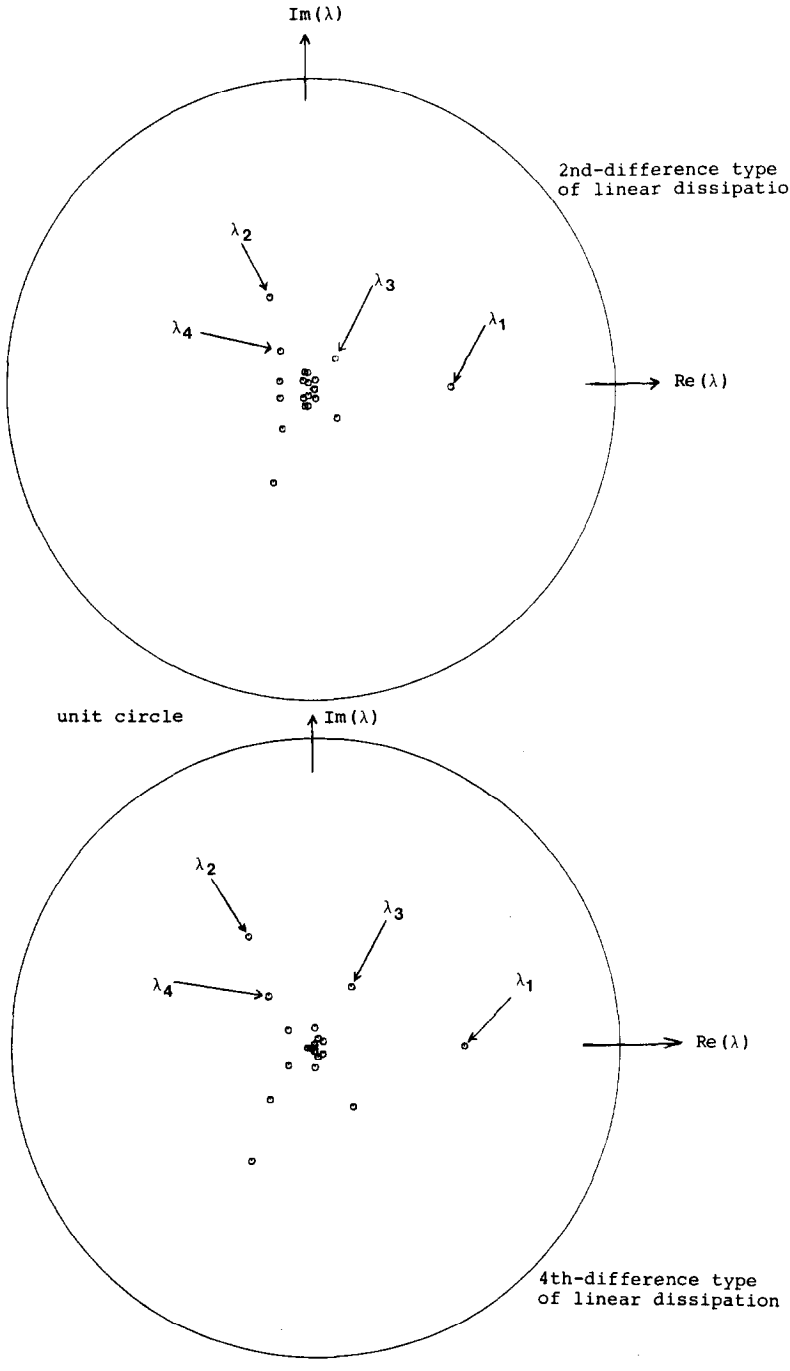

FIG. 5a. Spectrum of transformed linearized system. Transformation defined by $D(\Delta t, l) = (I + \Delta t A + \frac{1}{2}\Delta t^2 A^2 + \frac{1}{4}\Delta t^3 A^3)^l$ for $\Delta t = 0.9\Delta t_{max}$, $l = 50$, 32×7 mesh around NACA 0012 airfoil, $M_\infty = 0.8$, $\alpha = 0°$, both nonlinear and linear dissipation added. System linearized around solution shown in Fig. 4.

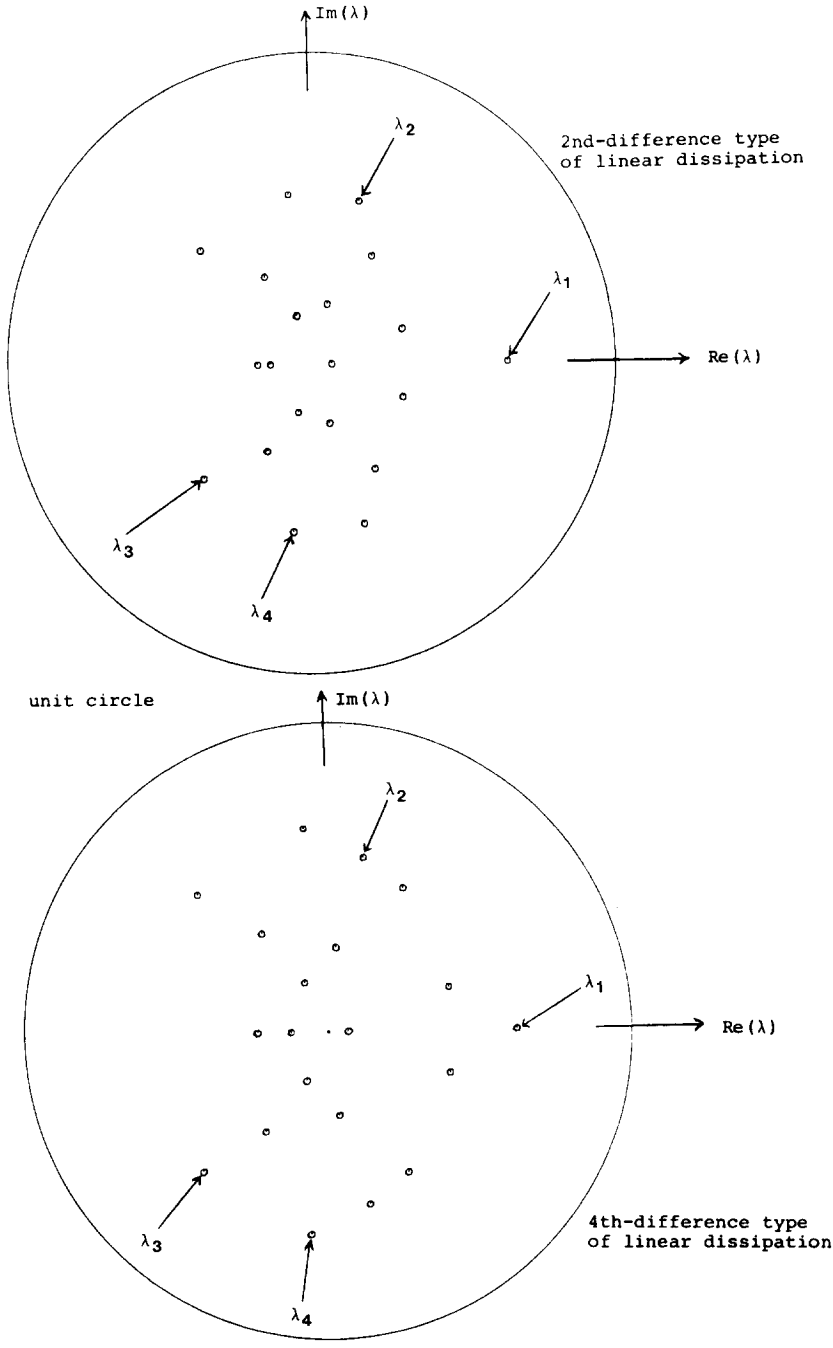

FIG. 5b. Same as Fig. 5a but for the 64 × 14 mesh.

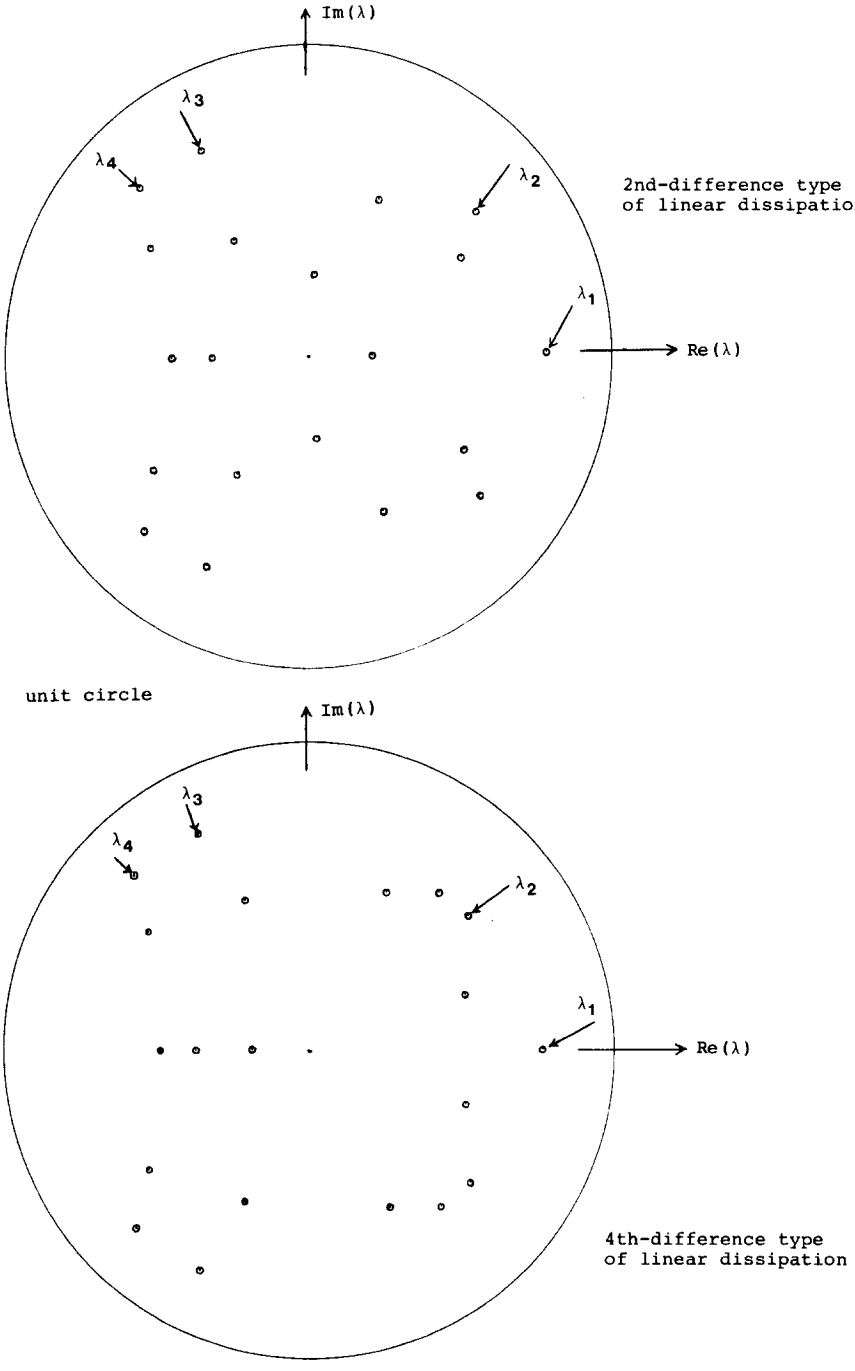

FIG. 5c Same as Fig. 5a but for the 128 × 28 mesh.

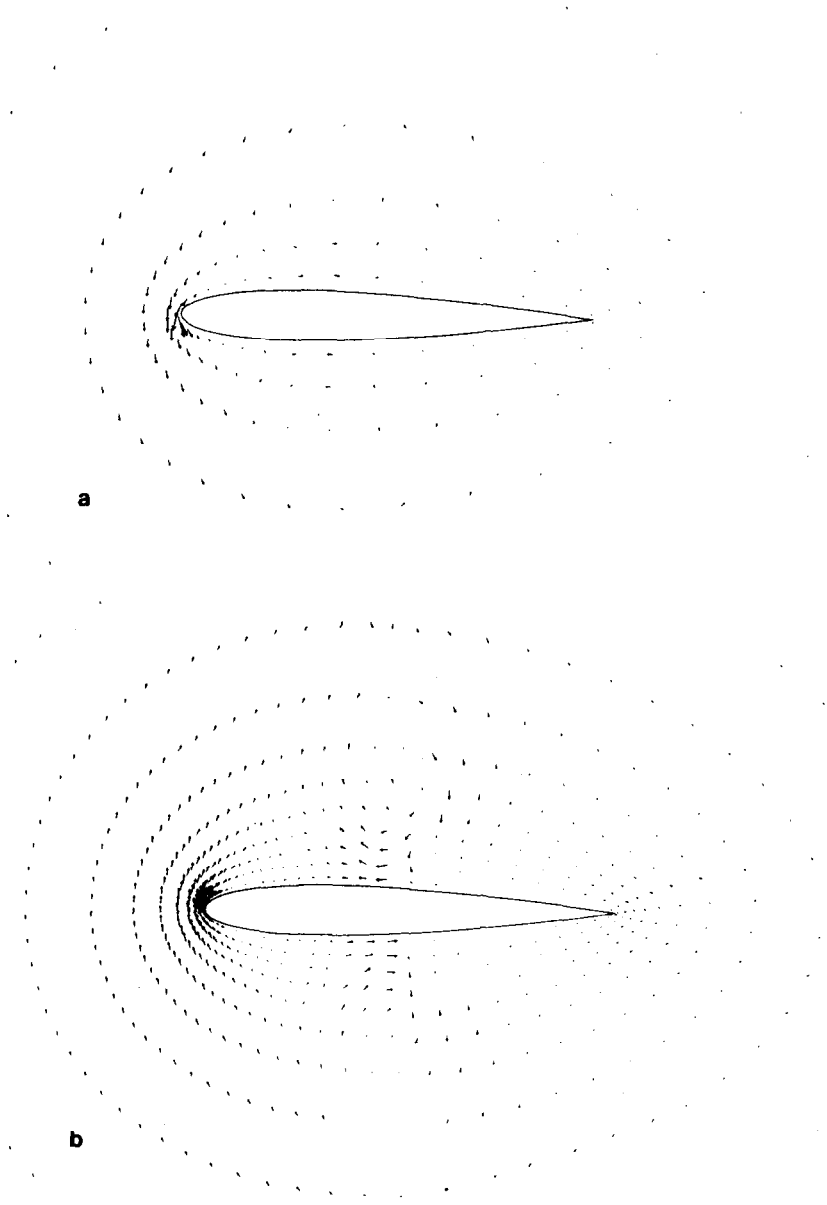

FIG. 6a. Eigenmode corresponding to eigenvalue λ_1 (in Fig. 5a) on 32×7 mesh, second-difference type of linear dissipation.

FIG. 6b. Eigenmode corresponding to eigenvalue λ_1 (in Fig. 5b) on 64×14 mesh, second-difference type of linear dissipation.

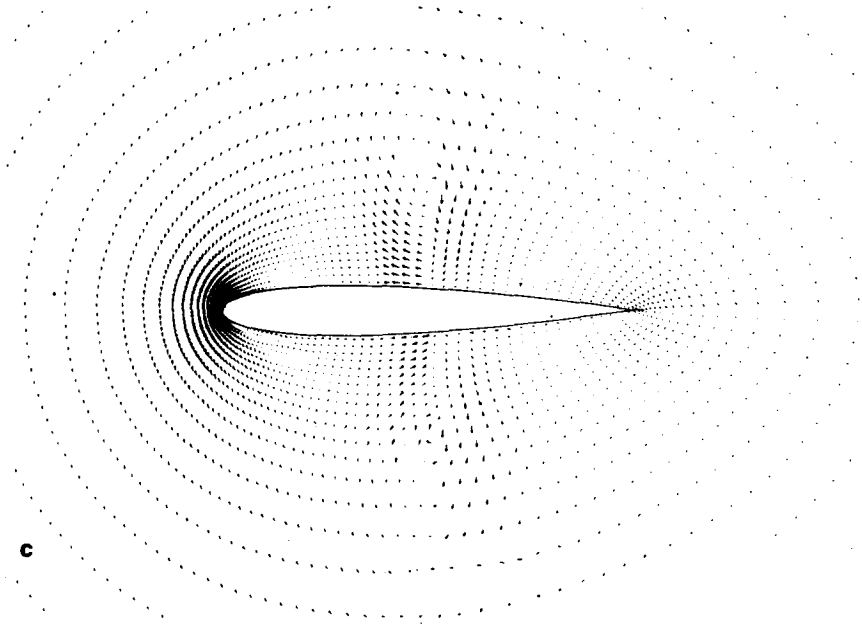

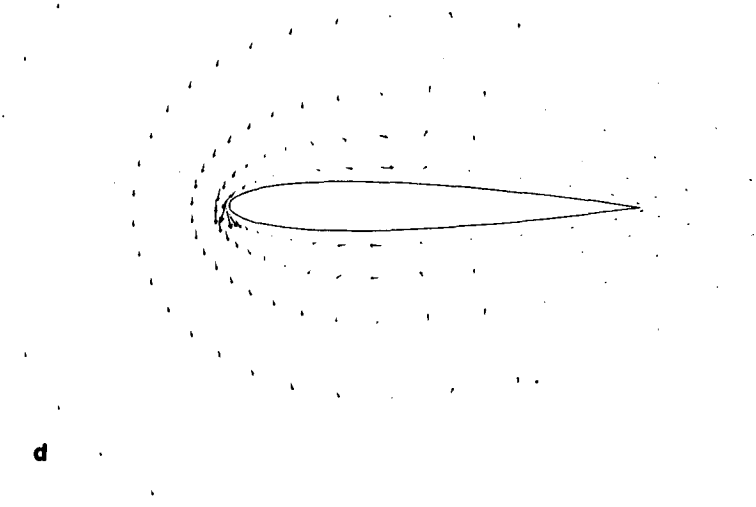

FIG. 6c. Eigenmode corresponding to eigenvalue λ_1 (in Fig. 5c) on 128×28 mesh, second-difference type of linear dissipation.

FIG. 6d. Eigenmode corresponding to eigenvalue λ_1 (in Fig. 5a) on 32×7 mesh, fourth-difference type of linear dissipation.

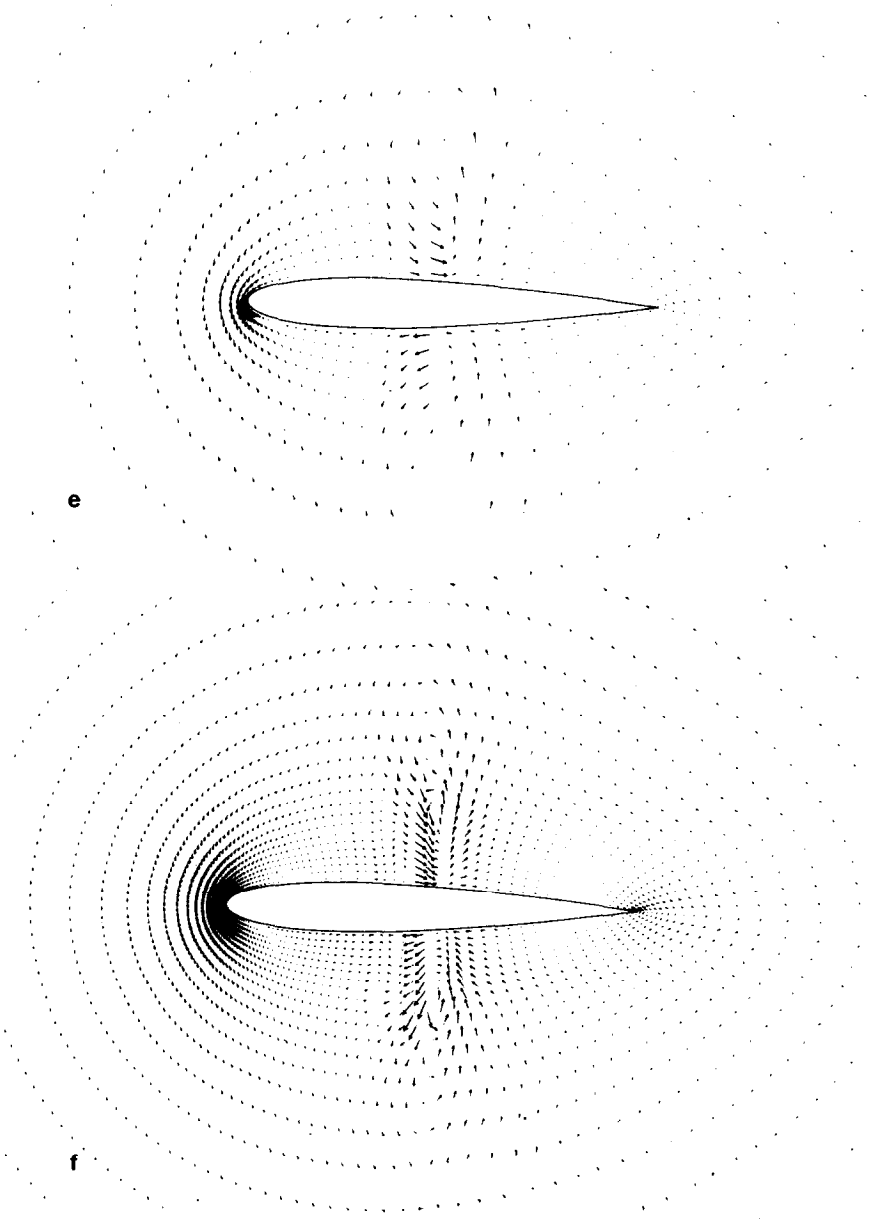

FIG. 6e. Eigenmode corresponding to eigenvalue λ_1 (in Fig. 5b) on 64×14 mesh, fourth-difference type of linear dissipation.

FIG. 6f. Eigenmode corresponding to eigenvalue λ_1 (in Fig. 5c) on 128×28 mesh, fourth-difference type of linear dissipation.

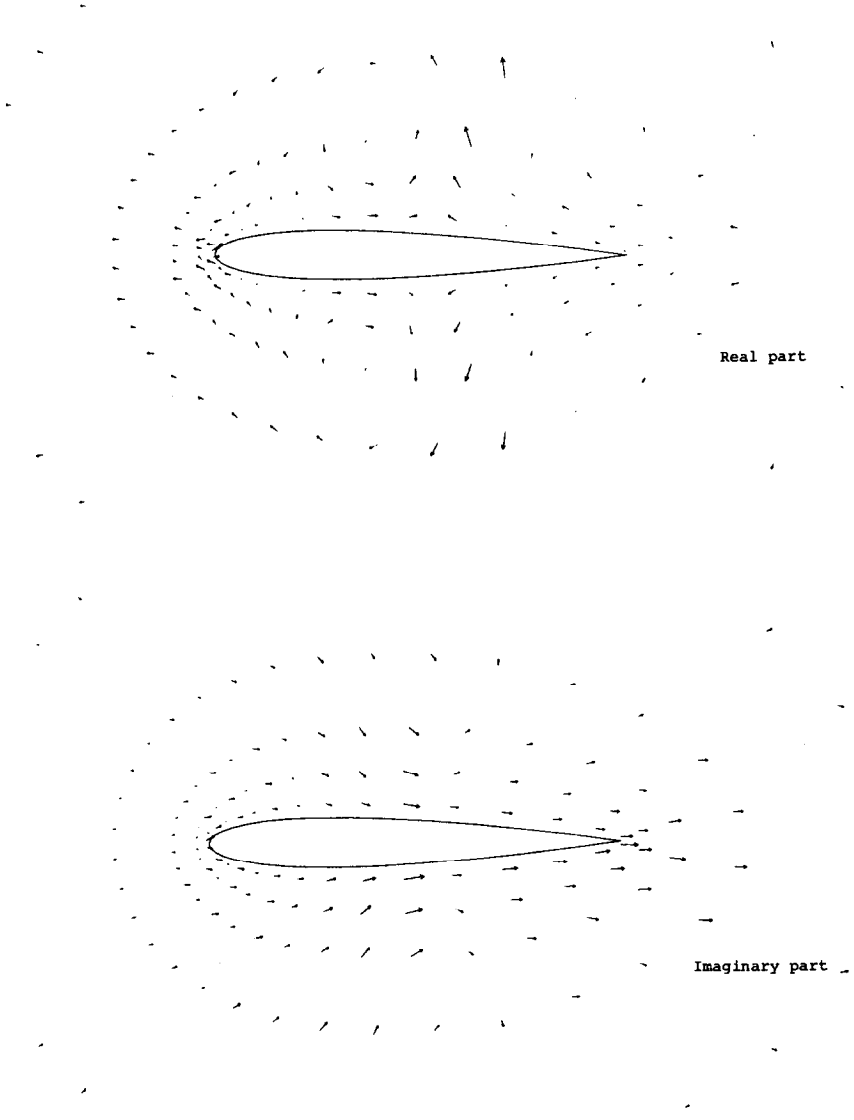

FIG. 7a. Eigenmode corresponding to eigenvalue λ_2 (in Fig. 5a) on 32×7 mesh, second-difference type of linear dissipation.

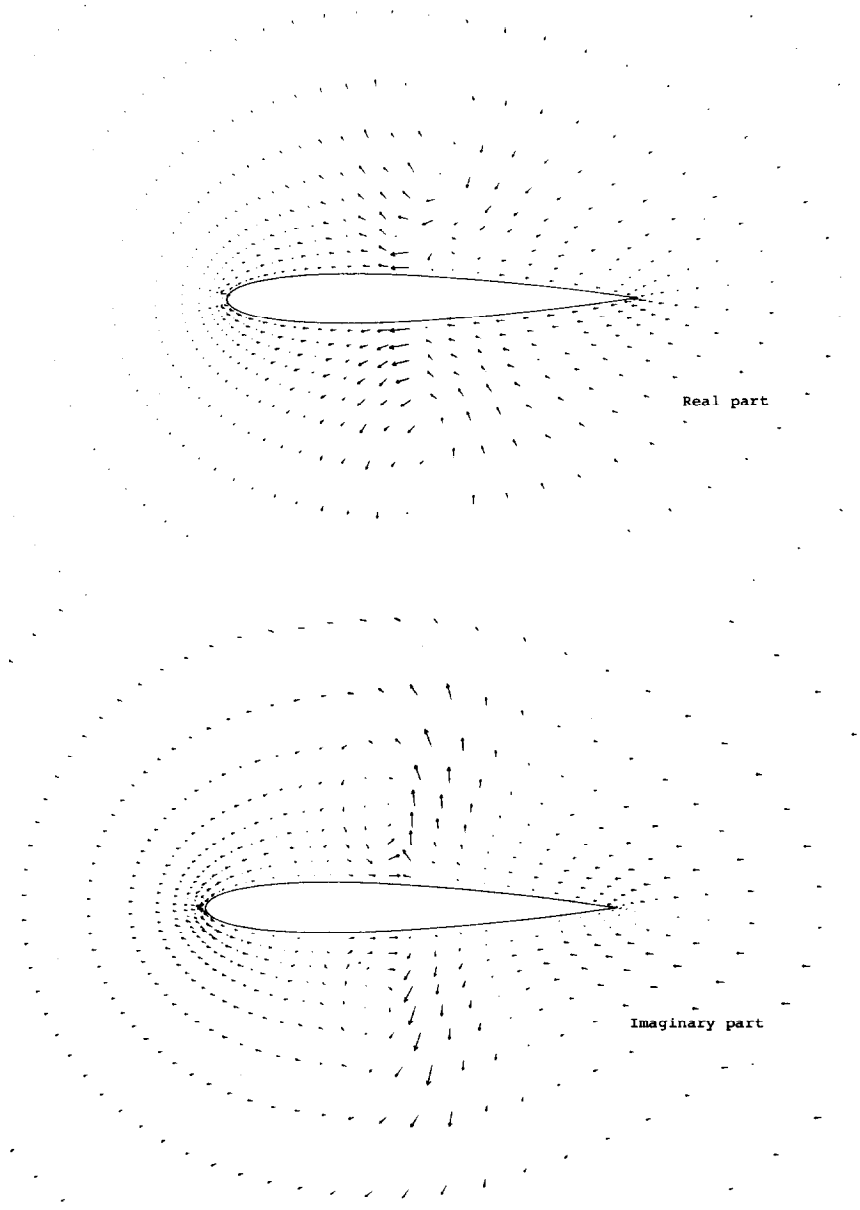

FIG. 7b. Eigenmode corresponding to eigenvalue λ_2 (in Fig. 5b) on 64×14 mesh, second-difference type of linear dissipation.

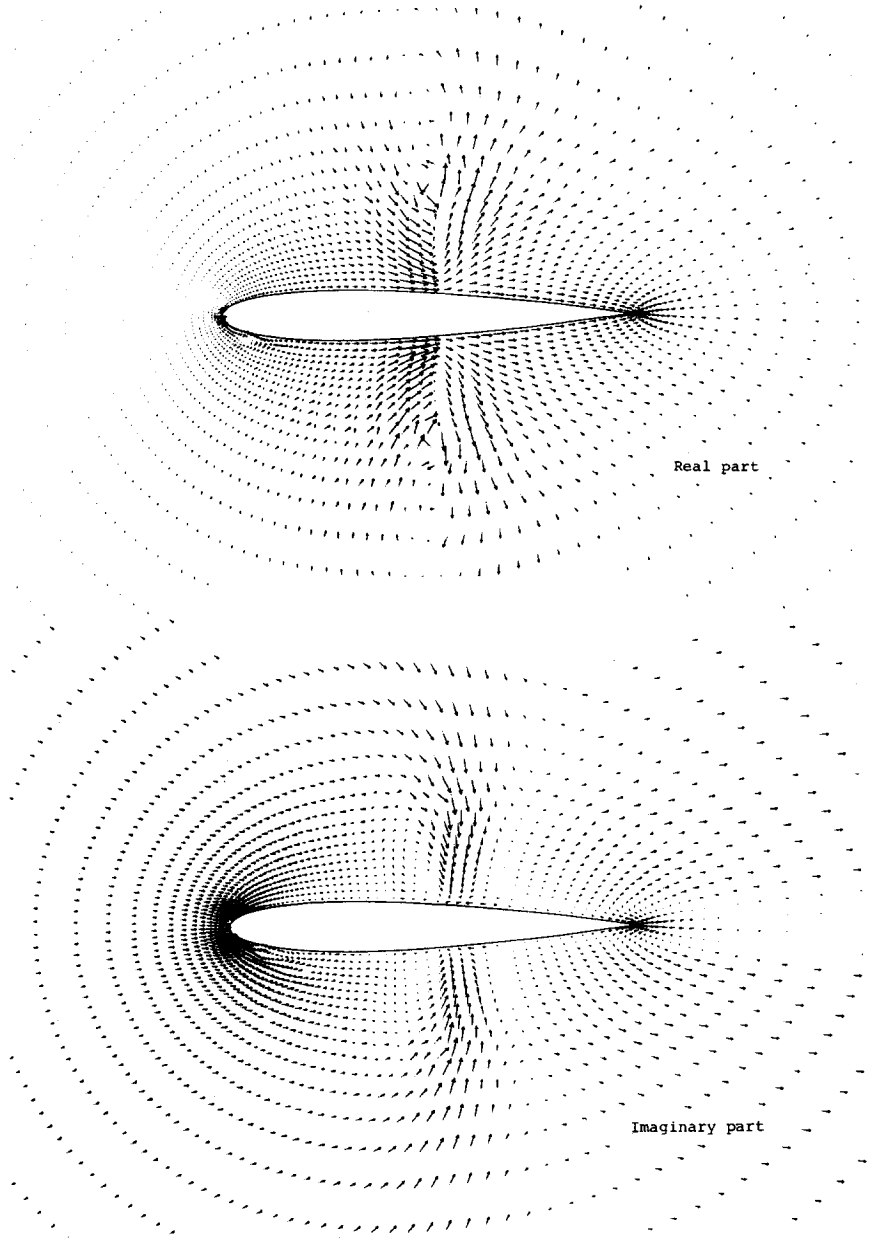

FIG. 7c. Eigenmode corresponding to eigenvalue λ_2 (in Fig. 5c) on 128×28 mesh, second-difference type of linear dissipation.

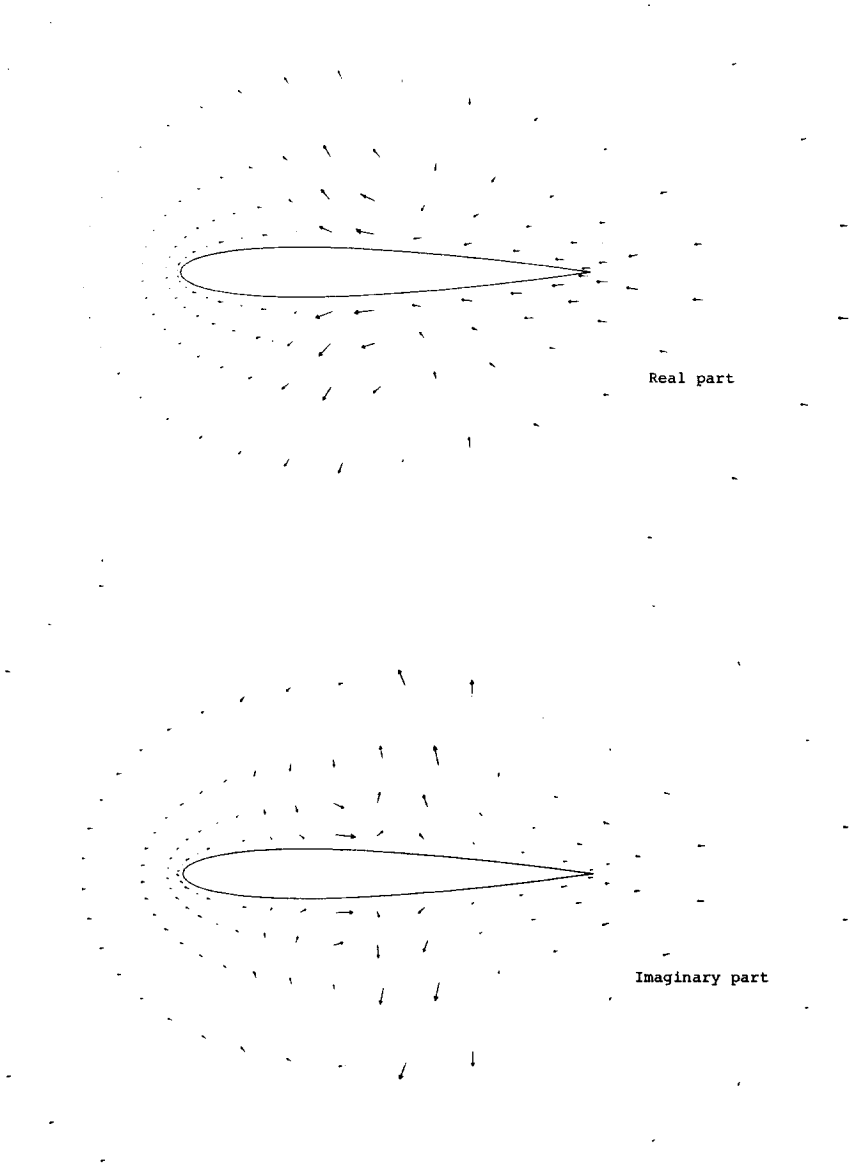

FIG. 7d. Eigenmode corresponding to eigenvalue λ_2 (in Fig. 5a) on 32×7 mesh, fourth-difference type of linear dissipation.

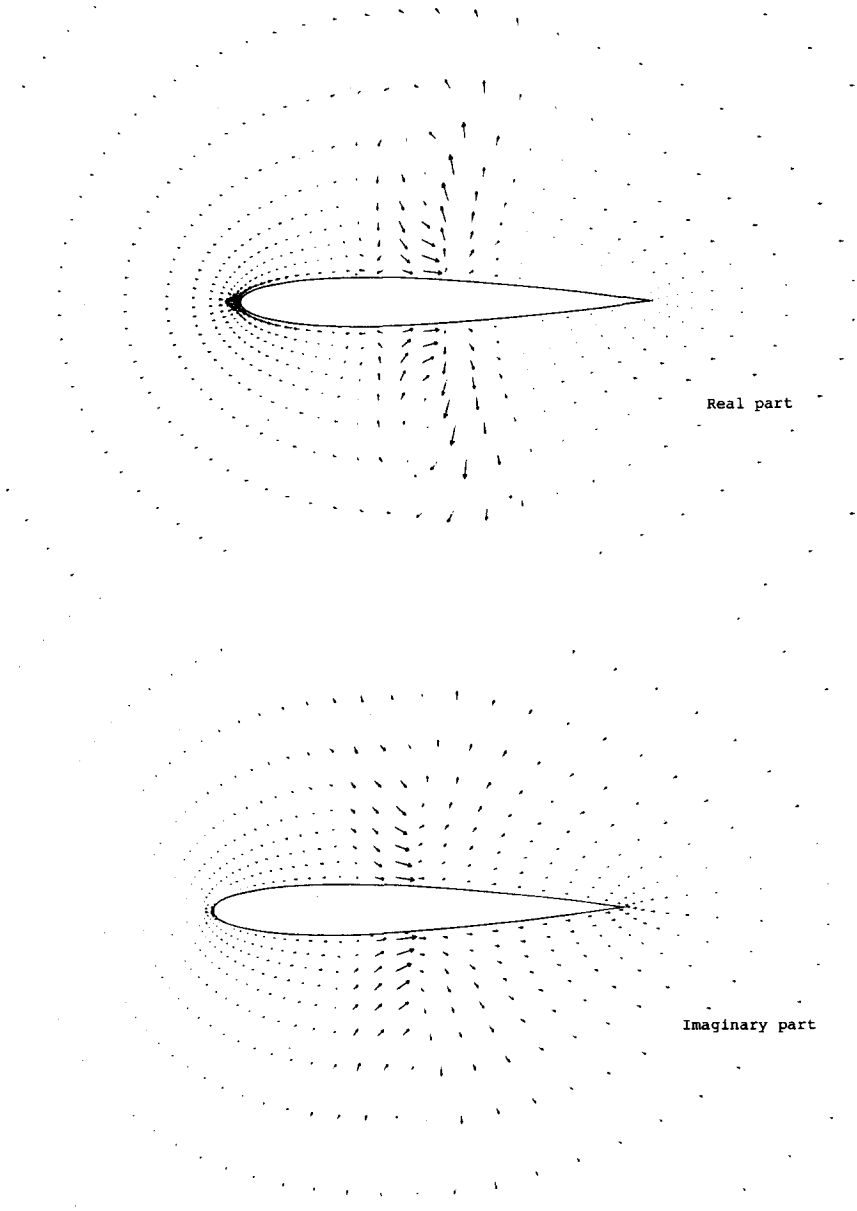

FIG. 7e. Eigenmode corresponding to eigenvalue λ_2 (in Fig. 5b) on 64×14 mesh, fourth-difference type of linear dissipation.

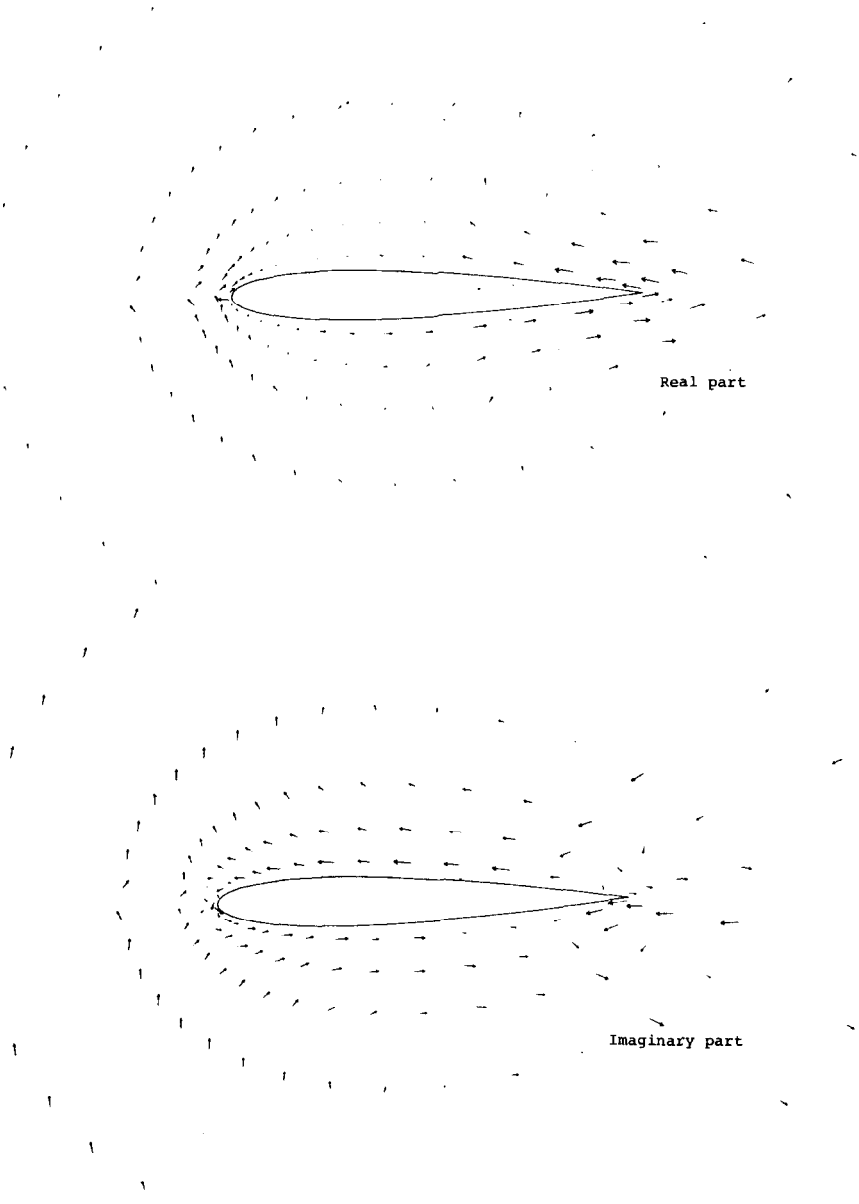

FIG. 8a. Eigenmode corresponding to eigenvalue λ_3 (in Fig. 5a) on 32×7 mesh, second-difference type of linear dissipation.

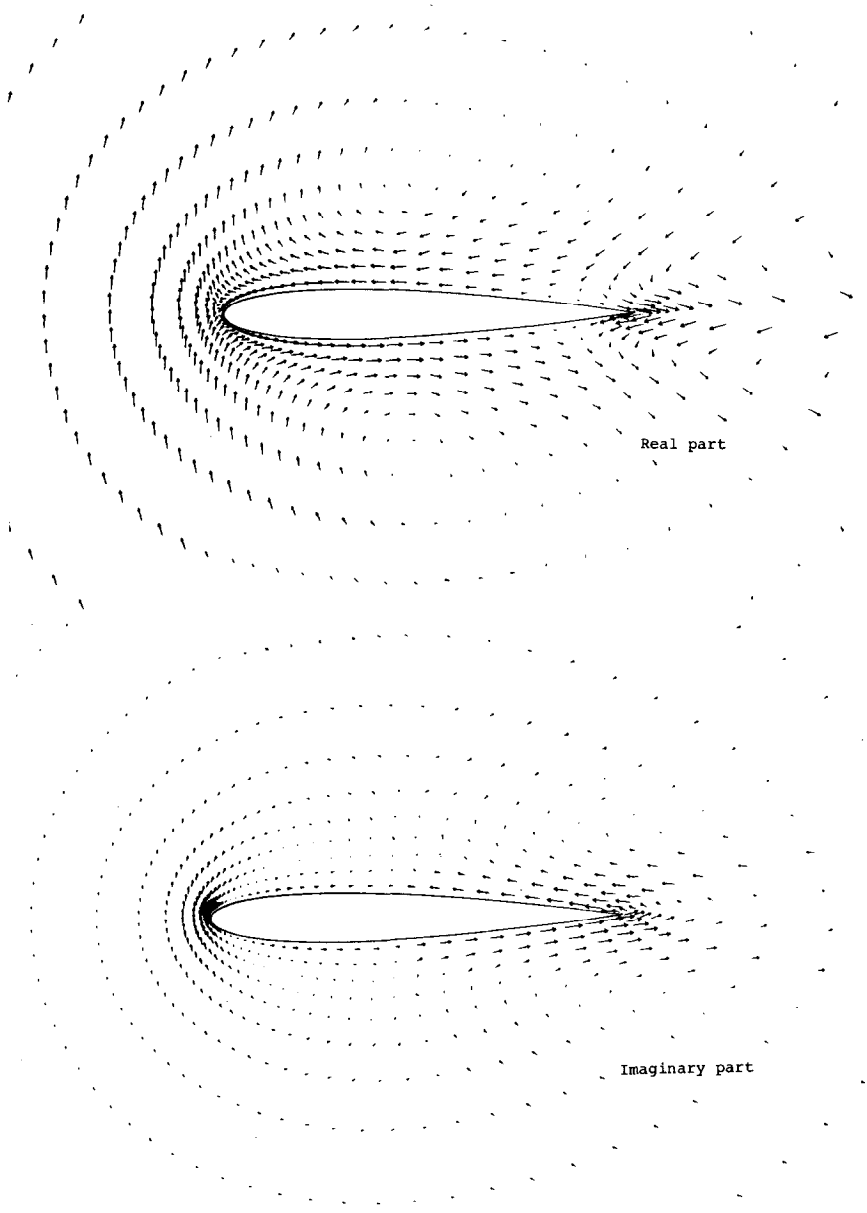

FIG. 8b. Eigenmode corresponding to eigenvalue λ_3 (in Fig. 5b) on 64×14 mesh, second-difference type of linear dissipation.

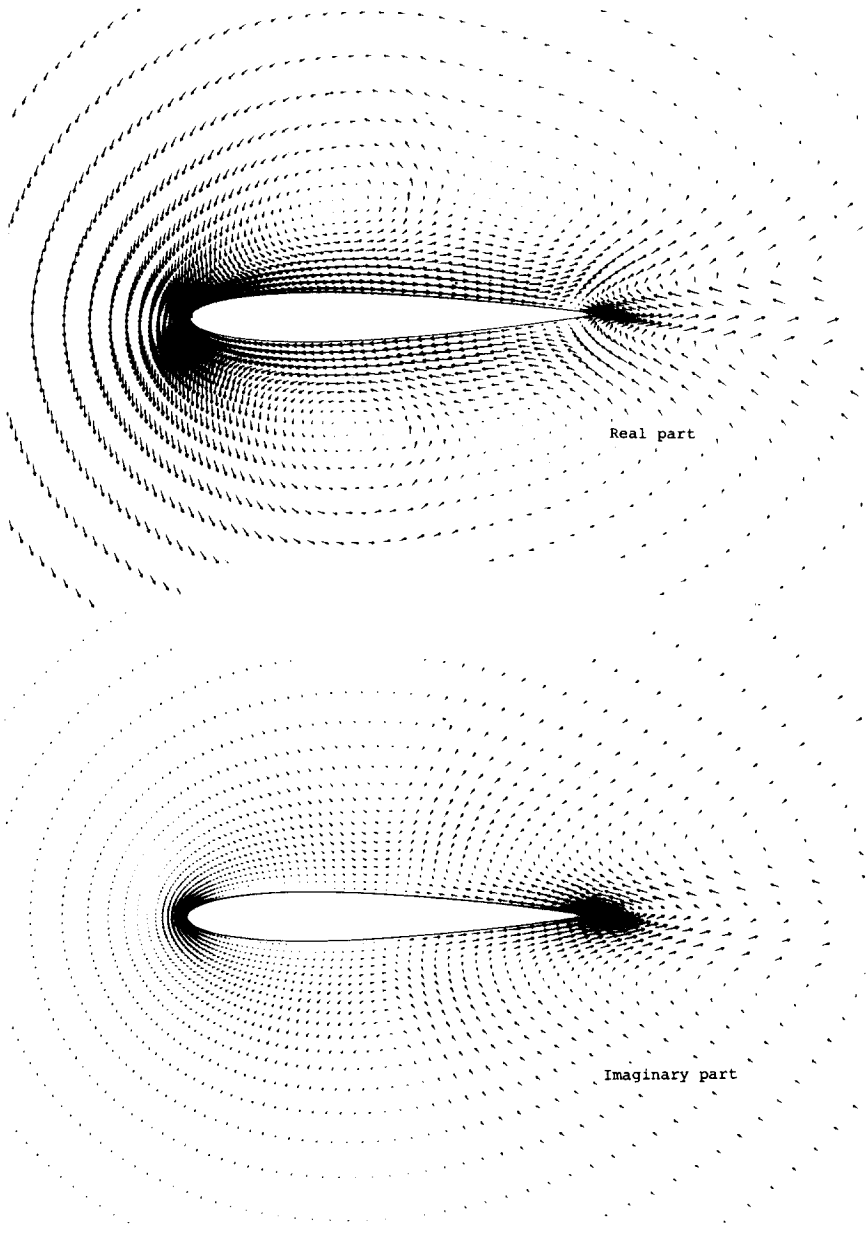

FIG. 8c. Eigenmode corresponding to eigenvalue λ_3 (in Fig. 5c) on 128×28 mesh, second-difference type of linear dissipation.

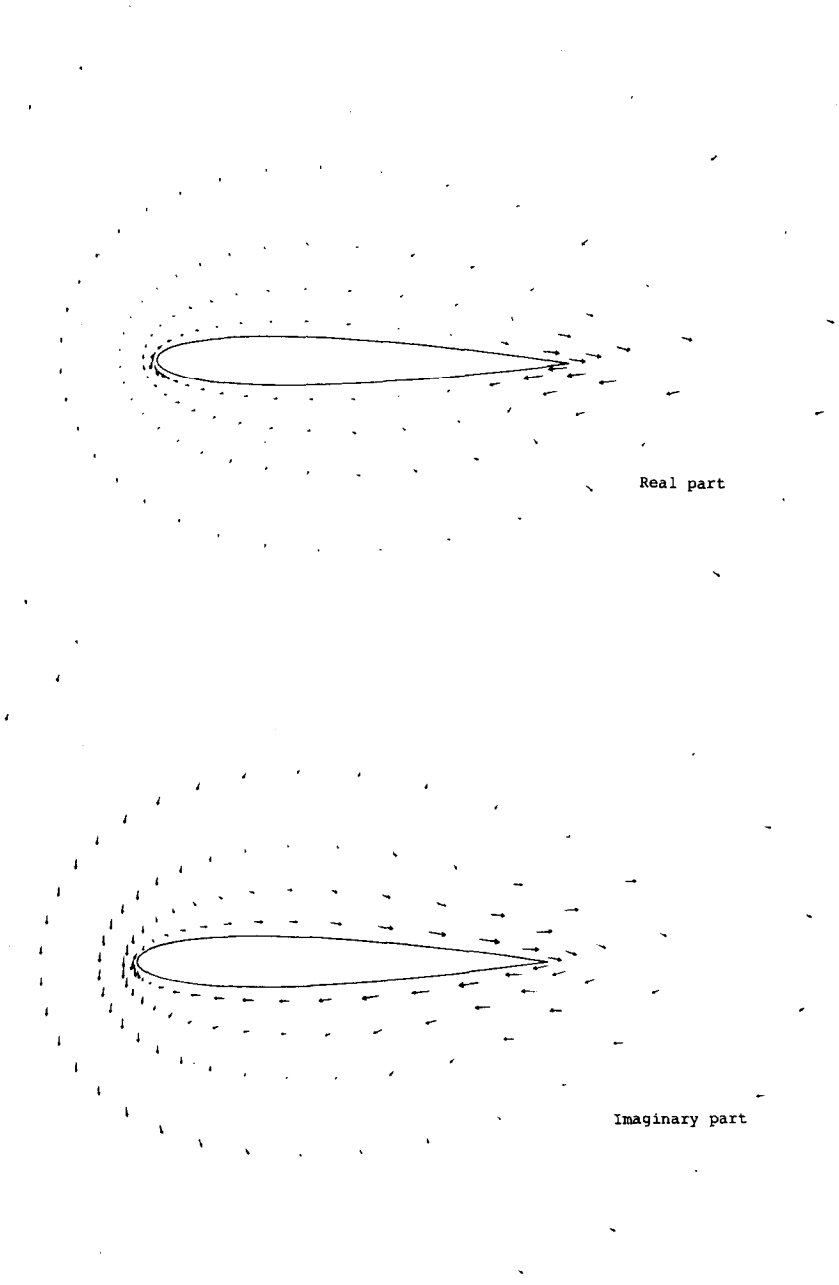

FIG. 8d. Eigenmode corresponding to eigenvalue λ_3 (in Fig. 5a) on 32×7 mesh, fourth-difference type of linear dissipation.

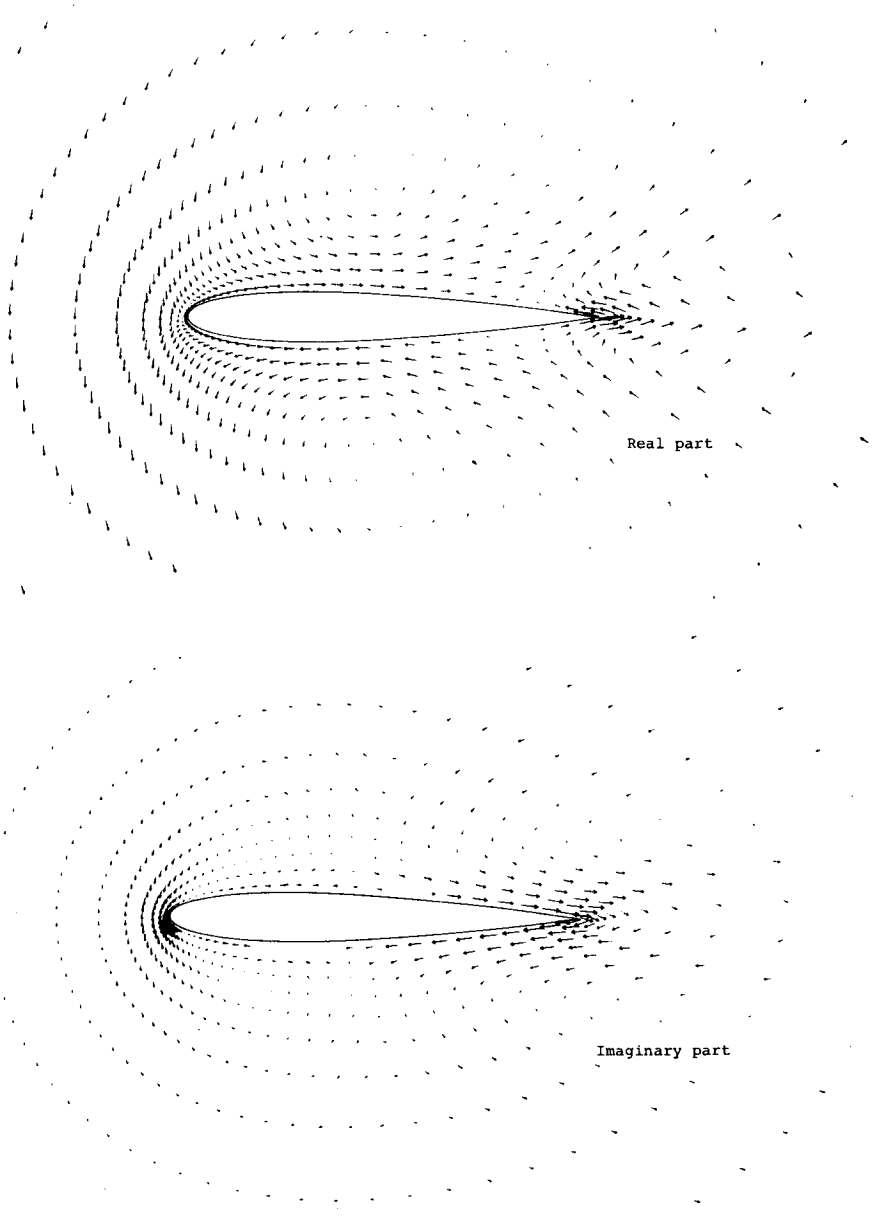

FIG. 8e. Eigenmode corresponding to eigenvalue λ_3 (in Fig. 5b) on 64×14 mesh, fourth-difference type of linear dissipation.

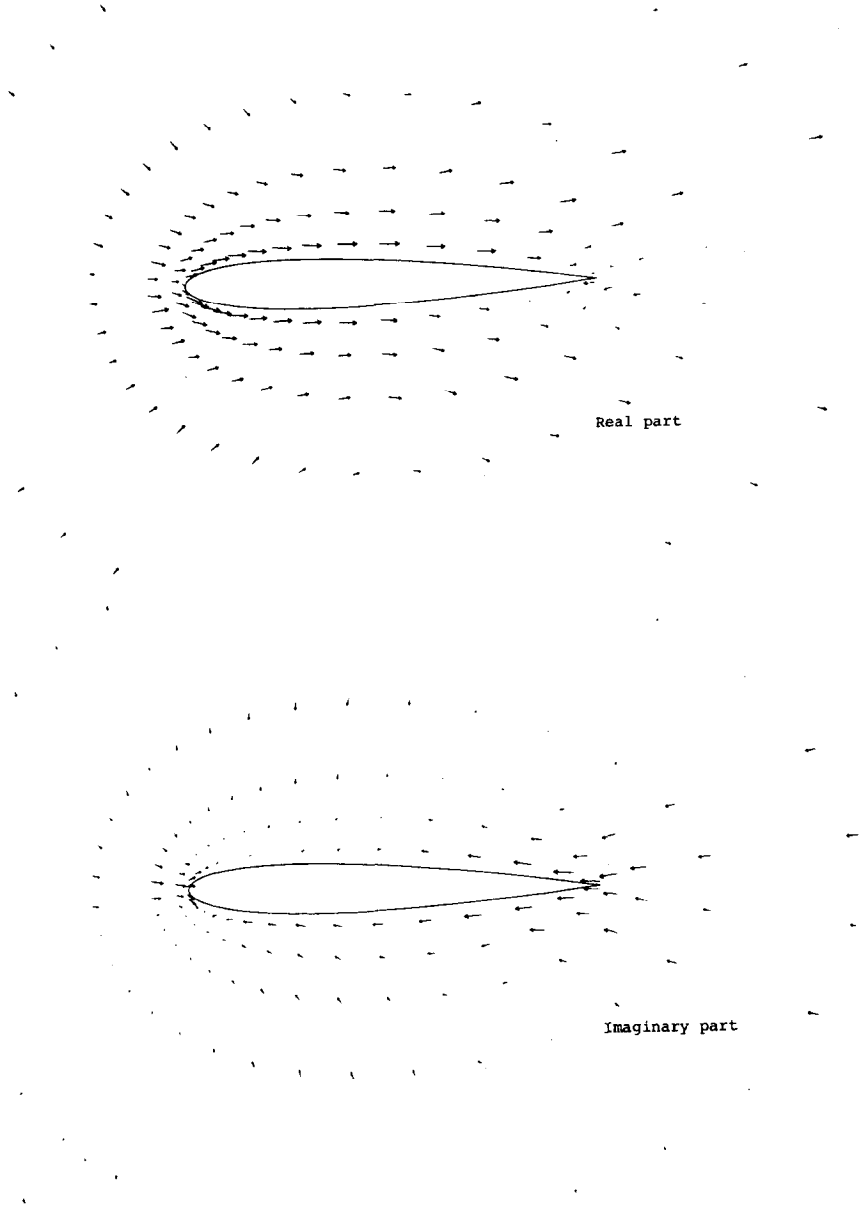

FIG. 9a. Eigenmode corresponding to eigenvalue λ_4 (in Fig. 5a) on 32×7 mesh, second-difference type of linear dissipation.

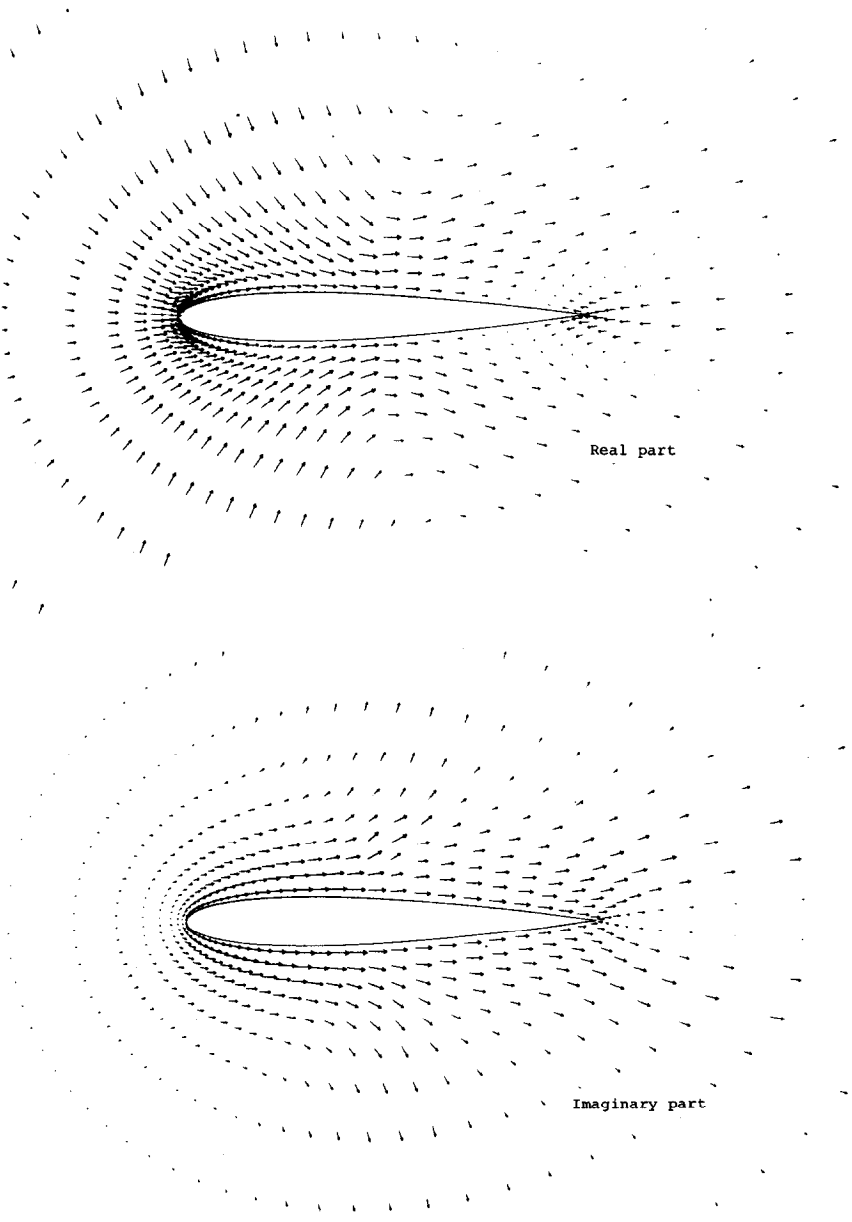

FIG. 9b. Eigenmode corresponding to eigenvalue λ_4 (in Fig. 5b) on 64×14 mesh, second-difference type of linear dissipation.

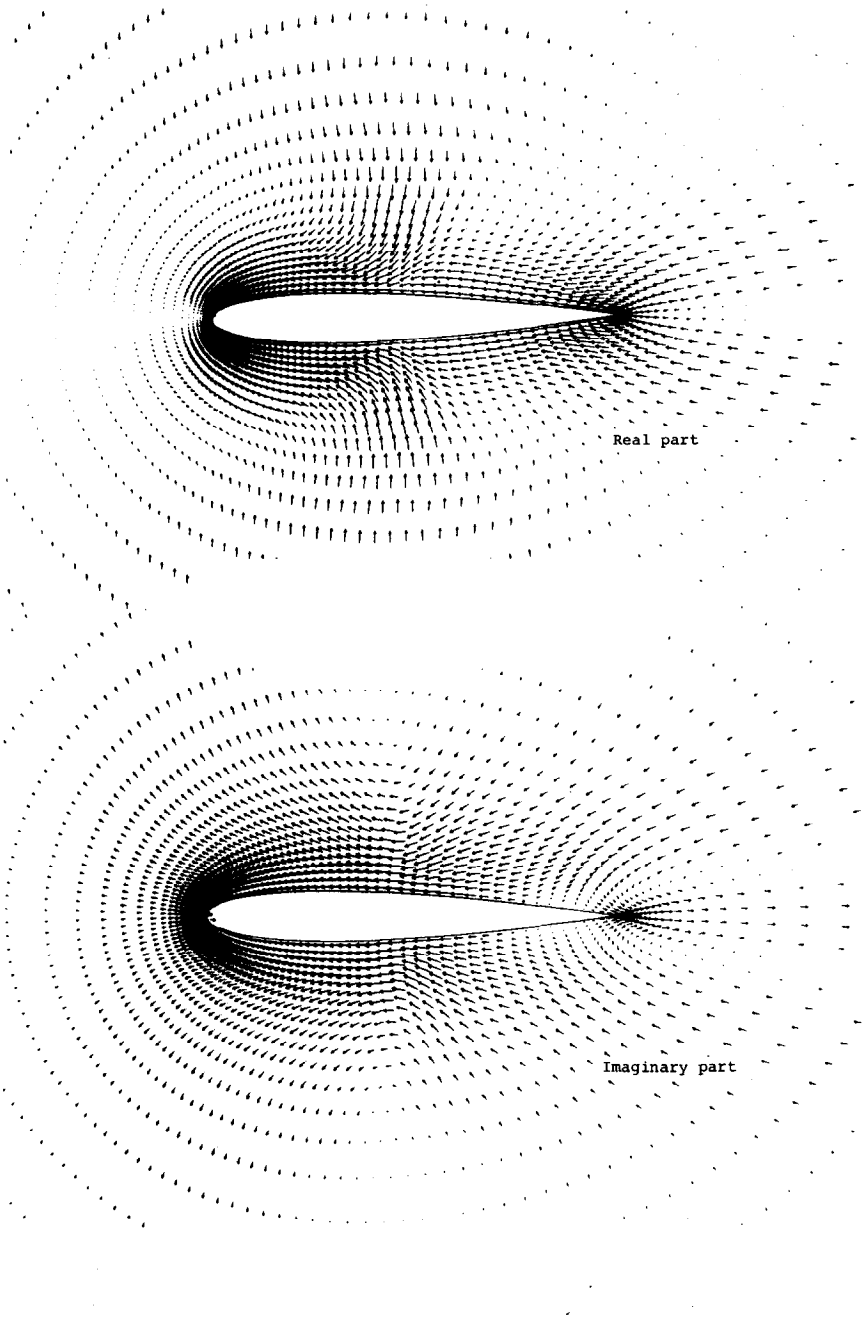

FIG. 9c. Eigenmode corresponding to eigenvalue λ_4 (in Fig. 5c) on 128×28 mesh, second-difference type of linear dissipation.

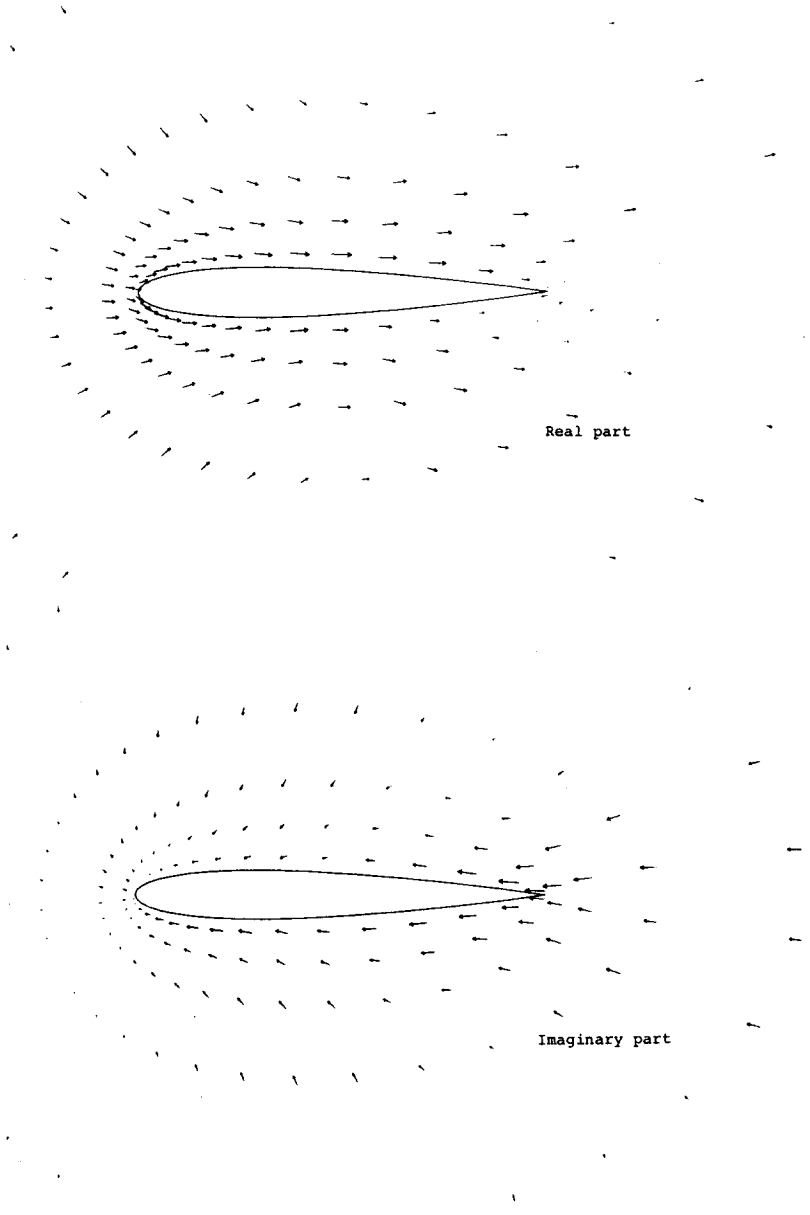

FIG. 9d. Eigenmode corresponding to eigenvalue λ_4 (in Fig. 5a) on 32×7 mesh, fourth-difference type of linear dissipation.

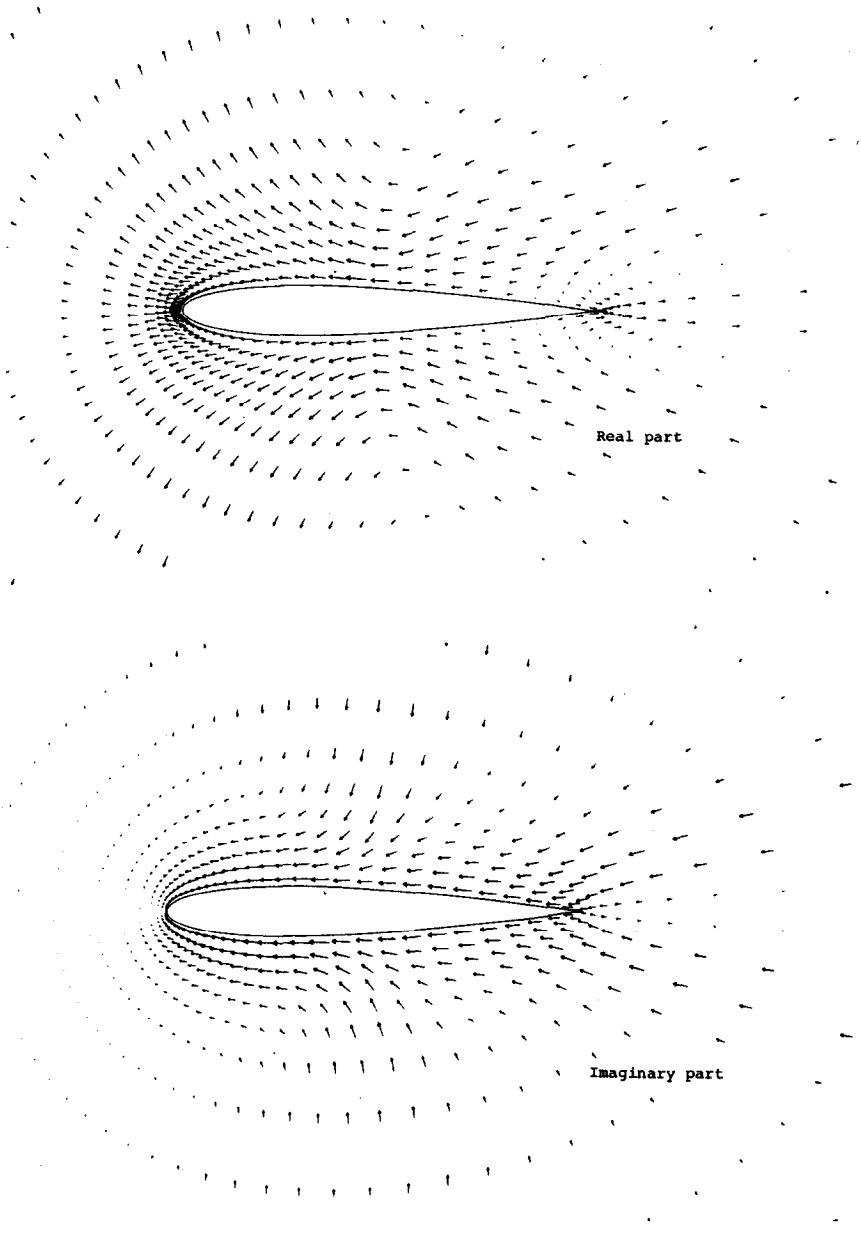

FIG. 9e. Eigenmode corresponding to eigenvalue λ_4 (in Fig. 5b) on 64×14 mesh, fourth-difference type of linear dissipation.

the most persistent modes is minor. It should be mentioned that in all cases, several runs with the approximate eigenvalue procedure have been made with different random starting vectors to confirm the accuracy of the least damped eigenvalues and their corresponding eigenvectors.

As the spectra in Figs. 5a–c show, one of the least damped modes has a real eigenvalue in all six cases (λ_1). The structure of this eigenmode is shown in Figs. 6a–c for the second-difference type of linear artificial viscosity and in Figs. 6d–f for the fourth-difference type of linear artificial viscosity (visualized by plotting the x- and y-components of the momentum perturbation at each grid point.) Even though this mode can be identified on all three meshes, it is obvious that it is of the type discussed above; i.e., it is so highly structured that it is near the resolution limit of each mesh. The fact that this effect is more pronounced in the case of fourth-difference linear dissipation must be due to the sharper shock in the steady solution that this partcular combination of viscosity allows (see Fig. 4). A closer look at Fig. 6f actually gives a hint of the "meaning" of this eigenmode. The areas where the eigenmode has large parturbations coincide with the shock region and the stagnation region of the airfoil. Since the mode clearly is antisymmetric with respect to the upper and lower half of the physical domain, it is evident that it represents an antisymmetric perturbation of the shock position and an accompanying perturbation of the position of the stagnation point. It is perhaps not surprising that this type of shock motion, which affects the overall circulation around the airfoil, is among the least damped modes.

Another eigenmode that has been identified on all three meshes is associated with eigenvalue λ_2 in Figs. 5a–c. The corresponding eigenmodes are shown in Figs. 7a–c for the second-difference type of linear viscosity and in Figs. 7d, 7e for the fourth-difference type of linear viscosity (the fine mesh fourth-difference linear viscosity case is not shown because this mode was not satisfactorily resolved.) This mode is clearly symmetric with respect to the upper and lower half of the domain and also has its greatest perturbations in the shock region of the airfoil. In contrast to the first mode, this eigenmode can be interpreted as a symmetric perturbation of the shock position (and strength). It should be noted that the comparison of complex eigenvectors is rather difficult because the representation of such an eigenvector by a "real" part and an "imaginary" part is not unique. The particular representation that comes out from the approximate eigenvalue procedure depends on the starting vector used. Since we use completely random starting vectors in all cases, it is to be expected that the resulting representations of the computed complex eigenmodes are different. This fact must be kept in mind when comparing the various complex eigenmodes shown.

The two eigenmodes shown so far are primarily connected to the shock region and stagnation region of the airfoil. Another type of eigenmode that seems to be connected to the trailing edge of the airfoil is shown in Figs. 8a–c (for the second-difference type of linear dissipation) and Figs. 8d,e (for the fourth-difference type of linear dissipation). This antisymmetric eigenmode corresponds to the eigenvalue marked λ_3 in Figs. 5a–c and is highly structured in the wake region of the airfoil. It seems that the sharp trailing edge of the airfoil is responsible for this shearing type of

transient mode which surprisingly stretches very far downstream. The widening of the wake region in the downstream direction that can be observed is very likely caused by the increased mesh cell size in that direction typical of all 0-type meshes.

A symmetric eigenmode that also displays a marked structure in the wake region is shown in Figs. 9a–c (for the second-difference type of linear dissipation) and Figs. 9d,e (for the fourth-difference type of linear dissipation). This eigenmode corresponds to the eigenvalue marked λ_4 in Figs. 5a–c.

The typical persistent eigenmodes shown so far have in common the fact that they are highly structured in the sense that the resolving power of each mesh is used to the limit. This means that the approximation of such a persistent eigenmode on a coarser mesh is at best a difficult and sensitive task.

4.3. *Efficiency of Linear Artificial Viscosity*

The initial results discussed in Section 4.1 showed the beneficial effect of a global linear artificial viscosity on the smoothness of the most persistent eigenmodes on the coarse mesh (32×7). These preliminary results were obtained for a second-difference type of linear dissipation. The later results discussed in Section 4.2 for both the second-difference and the fourth-difference type of linear dissipation provide additional information concerning the merits of these two different viscosity models. For example, a comparison of the eigenmodes shown in Figs. 7b and 7e demonstrates the difference between the two viscosity models. It is evident from this comparison that the fourth-difference type of linear artificial viscosity is more effective than the second-difference type in eliminating saw-tooth patterns in the eigenmodes. Furthermore, as the steady solutions in Fig. 4 show, the fourth-difference linear viscosity model can be combined with the nonlinear second-difference type of viscosity in such a way that the shocks are reasonably sharp.

5. Conclusions

The fact that the most persistent eigenmodes of the linearized system are highly structured and therefore tax the resolving power of all meshes to the limit calls into question the ability of any conventional multi-grid method to work effectively on them. It seems likely that any such method to accelerate the convergence to steady state must be able to act on these modes through a projection process onto a suitable subspace. The difficulty lies in the construction of such a subspace without excessive computational effort. In the usual multi-grid method, the subspace construction is very simple (= the next coarser mesh) and does not require any large computational effort, but the resulting subspace obviously cannot resolve highly structured eigenmodes with sufficient detail. Other methods, for example Krylov subspace methods, rely on the solution process itself to generate a suitable subspace on which to project the persistent modes and damp them quickly. Their main disadvantage is that they often require a large computational effort and/or large computer memory. We have just read of Jameson and Baker's very recent success with a multigrid

method for the Euler equations [8]. Although the convergence rates they have obtained in several transonic flow examples are not as rapid as those now commonly achieved when solving the potential equation by multigrid, they have undeniably demonstrated an effective improvement by multigrid in the convergence to the steady state of those hyperbolic equations. The success of their scheme (they say) is critically dependent on the temporal damping of their multistage time integration, and they go to some effort to optimize it to eliminate short waves. It may be that their most persistent modes are smoother than the ones we found for our scheme, and their method therefore can work effectively on these in the coarse mesh. But the only way to really understand it, of course, is to analyze the eigenproperties of this multigrid scheme with the procedure described here.

We should also emphasize that our eigensystem analysis is a versatile tool not limited only to studying asymptotic convergence but proving useful as an instrument to compare critically various concepts of boundary conditions and artificial viscosity models by bringing out their different effects in the quantitative detail of their eigensystem decomposition. It may even tell us something about the quality of computational meshes, i.e., the relative strengths and weaknesses of different mesh densities, spacing, and topology. Furthermore, it is general in the sense that it can analyze any method. Given a flow-solving code all one needs to do is to create a solution field about which to linearize and then in a simple modular way insert into the analysis program the flow-solver's subroutine that forms its flux quantities at every grid point in the field. The rest is done by computer. We should not, however, belittle the computer's part. While the structure and basic concepts of our analysis program are simple and straightforward, it presents the machine with a great amount of computational work. For example to obtain the eigen-decomposition of the fine grid solution, our VAX 11/780 had to labor 16 hours.

REFERENCES

1. H. LOMAX, T. H. PULLIAM, AND D. C. JESPERSEN, "Eigensystem Analysis Techniques for Finite-Difference Equations. I. Multilevel Techniques," AIAA Paper 81–1027, 1981.
2. A. RIZZI, AND L. E. ERIKSSON, *in* "Proceedings, 8th International Conference on Numerical Methods in Fluid Dynamics," (E. Krause, Ed.), Lecture Notes in Physics, Springer-Verlag, New York/Berlin, 1982.
3. L. E. ERIKSSON, "A Study of Mesh Singularities and Their Effects on Numerical Errors," FFA Tech. Note TN 1984-10, Stockholm, 1984.
4. J. D. DENTON, *in* "Numerical Methods in Applied Fluid Dynamics," (B. Hunt, Ed.), Academic Press, New York/London, 1980.
5. W. E. ARNOLDI, *Quart. Appl. Math.* **9** (1951), 17–29.
6. Y. SAAD, *Linear Algebra Appl.* **34** (1980), 269–295.
7. J. GARY, *Math. Comp.* **18** (1964), 1–18.
8. A. JAMESON, AND T. BAKER, AIAA Paper 84–0093, New York, 1984.

[1] Software availability: Readers interested in running this analysis program for themselves are invited to write to the authors for details.